ABSTRACT

Title of Thesis: IMPACT OF RIPPLE CURRENT ON X7R MULTILAYER CERAMIC CAPACITORS WITH BASE METAL ELECTRODES

Satwik Reddy Kommula,
Master of Science (M.Sc.), 2022

Thesis Directed By: Dr. Michael H. Azarian
Department of Mechanical Engineering

The trend towards miniaturization along with the availability of multilayer ceramic capacitors (MLCCs) in a wide range of voltage ratings and capacitances, makes MLCCs a viable option to be used in applications that were previously reserved for electrolytic capacitors. Capacitors are widely used in filtering applications that involves current flowing through them because of a varying voltage, which is known as ripple current. The power dissipated by the parasitic resistance (ESR) of the MLCCs raises its temperature when current flows through it. Operating under elevated temperatures over extended periods of time has the potential to degrade the performance of the MLCC resulting in a catastrophic failure or operating outside the limits. This study analyzes the performance of MLCCs when they are subjected to a varying voltage and compares the effects of different voltage ratings on the degradation of their electrical characteristics during extended exposure to ripple current. The failure mechanism for the degradation in insulation resistance observed in the tested MLCCs is also presented.

IMPACT OF RIPPLE CURRENT ON MULTILAYER CERAMIC CAPACITORS

by

Satwik Reddy Kommula

Thesis submitted to the Faculty of the Graduate School of the
University of Maryland, College Park, in partial fulfillment
of the requirements for the degree of
Master of Science
2022

Advisory Committee:
Dr. Michael H. Azarian, Chair
Professor Peter Sandborn
Professor Patrick McCluskey

Acknowledgements

I would like to thank my advisor, Dr. Michael H. Azarian, of Mechanical Engineer Department at the University of Maryland, College Park for guiding me in the correct direction throughout the term of the project. His support and motivation kept me focused and lead me to the successful completion of my project. Additionally, I would also like to thank Prof. Michael Pecht and Dr. Diganta Das.

I would like to thank Prof. Peter Sandborn and Prof. Patrick McCluskey for taking time and agreeing to be on the committee.

Finally, I must thank my parents and my friends for their love and support throughout.

Thank you.

Satwik Reddy Kommula.

Contents

List of Figures

List of Tables

1. Introduction to Multilayer Ceramic Capacitors

Capacitors are passive components that store energy in the form of electric field. Capacitors mainly consists of metal electrodes separated by a dielectric material between the electrodes, to increase the energy storage density. Figure 1 shows a basic construction of a capacitor consisting of two metal electrodes placed parallel to each other with a dielectric material separating the metal electrodes. The dielectric material is used to change the capacitance of the capacitors. Capacitance is given by:

$$C = \varepsilon \frac{n * a}{d} \text{ [1]}$$

Where, C is the capacitance, a is the area of the electrode, d is the distance between the electrodes and n is the number of electrodes

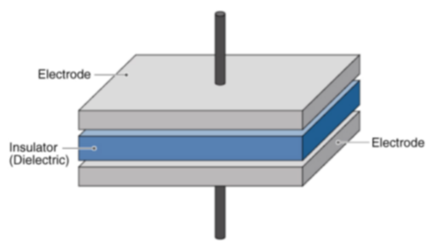

Figure 1 Construction of a capacitor [2]

Capacitors are classified depending on the dielectric material used, such as multilayer ceramic capacitors, aluminum electrolytic capacitors, tantalum electrolytic capacitors, and film capacitors [1]. Capacitors also come in a variety of sizes, shapes, voltage ratings and capacitance values. Capacitors are used for a number of applications including bypass capacitor, decoupling capacitor, filter capacitor and for many other purposes.

1.1 Multilayer Ceramic Capacitors (MLCCs)

Multilayer ceramic capacitors consist of multiple layers of metal electrodes stacked on each other with a ceramic dielectric material between the electrodes. Figure 2 shows the internal construction of MLCCs containing multiple layers of metal electrodes with ceramic dielectric material. Multilayer ceramic capacitors are available in many sizes ranging from 01005 to 8060 (EIA-198-inch code) [3] and with a wide range of voltage ratings and capacitance values. Figure 3 shows MLCCs of various case sizes.

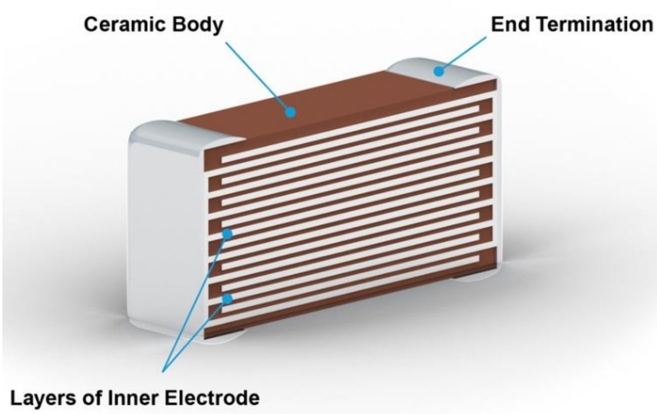

Figure 2 Construction of MLCCs [4]

MLCCs are further classified depending on the change in capacitance with external temperature and applied voltage. Three classes [3] of capacitors are identified ranging from no change in capacitance with applied conditions to extreme changes in capacitance with the applied conditions. Class I capacitors, also called are temperature compensating capacitors, are most stable, and the capacitance does not change with applied voltage and external temperature [3]. However, the capacitance values of class I capacitors are exceptionally low and cannot be used in applications requiring larger capacitance values.

Class II and III have high volumetric efficiency than class I MLCCs [3]. However, the capacitance of class II, III and IV changes with the applied voltage and operating temperature. The capacitance changes nonlinearly within the operating temperature, limiting the use of class II and III in applications requiring a strict capacitance requirement. Class II MLCCs are a capacitor of choice in applications requiring smaller case size and high volumetric efficiency and where slight change in capacitance is tolerable, such as in filtering applications, coupling, and decoupling signals.

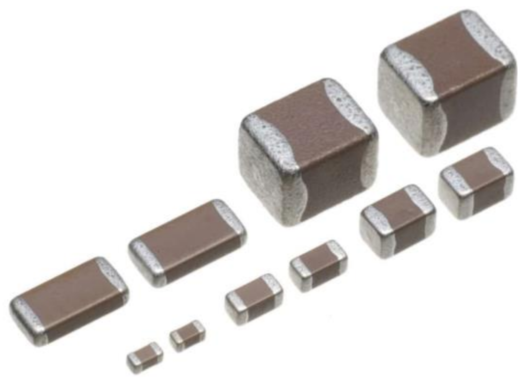

Figure 3 Multilayer ceramic capacitor

MLCCs offer the advantages of smaller case size, large voltage breakdown strengths, and good high frequency characteristics. The advantages of MLCCs along with availability in smaller case sizes and high volumetric efficiencies, make them a viable alternative to replace electrolytic capacitors that were traditionally used to filter the voltage fluctuations due to their high volumetric efficiency. Electrolytic capacitors are bulky and are less favorable towards miniaturization. Class II MLCCs, such as X7R, can potentially replace the electrolytic capacitors in applications requiring high volumetric efficiency and small form factor [5].

1.1.1 Phase Transformation in Barium Titanate

In class II MLCCs, the dielectric material used is barium titanate, which is doped to improve the temperature and voltage characteristics of the MLCCs. Below the Curie temperature (around 130°C), barium titanate exhibits a tetragonal structure in which one axis of the crystal lattice elongates, giving rise to dipoles [6] [7] [8]. The dipoles oriented in the same direction form domains. The domains are randomly distributed throughout the dielectric material resulting in high dielectric constant. Barium titanate exhibits ferroelectric properties and piezoelectric properties below the Curie temperature. The ratio of axis (c/a) keeps decreasing from 25°C to 120°C causing the capacitance to change even within the operating temperature range [7] [8] [9]. Over the Curie temperature, the barium titanate changes from tetragonal phase to cubic phase, resulting in the loss of dipoles and lower dielectric constant. In cubic phase, barium titanate is paraelectric in nature and loses its piezoelectric properties. Figure 4 shows the phase transformations of barium titanate at various temperatures.

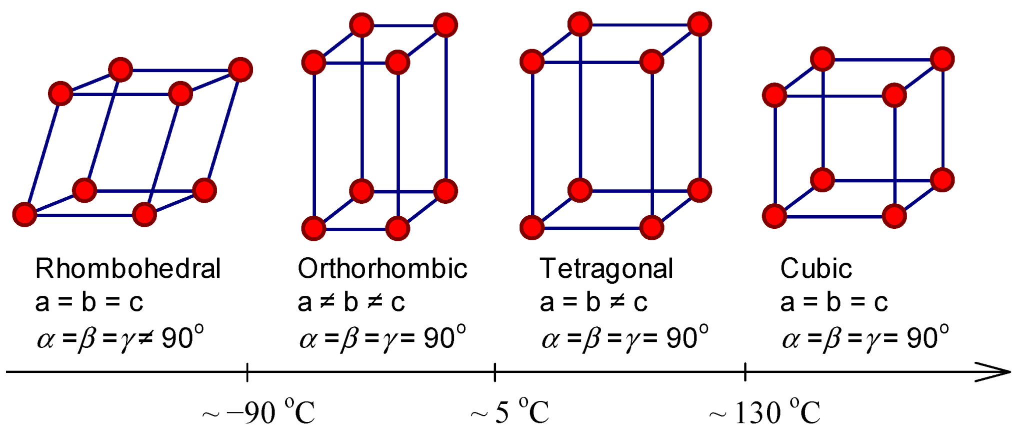

Figure 4 Phase transformations in barium titanate [10]

1.1.2 Manufacturing of Multilayer Ceramic Capacitors

The manufacturing of MLCCs start with the preparation of slurry consisting of the dielectric powder, solvents, dispersant, binder, and plasticizer. The slurry is then cast into a thin sheet. Electrode is then printed on the dried sheet of dielectric before stacking them layer by layer in a very precise fashion. The stacked laminate is then cut and diced before binder burnout to remove the organic components. To prevent the oxidation of the nickel electrodes used in class II MLCCs, the sintering process is conducted in reducing atmospheres and at a temperature of 1350°C. Sintering in the reduced atmospheres introduces oxygen vacancies in the bulk of the barium titanate. Attempts to reduce the number of oxygen vacancies by re-oxidation are conducted. The last step in the manufacturing process is to apply the termination and to perform electrical characterization [3]. Figure 5 shows the steps involved in the manufacture of MLCCs.

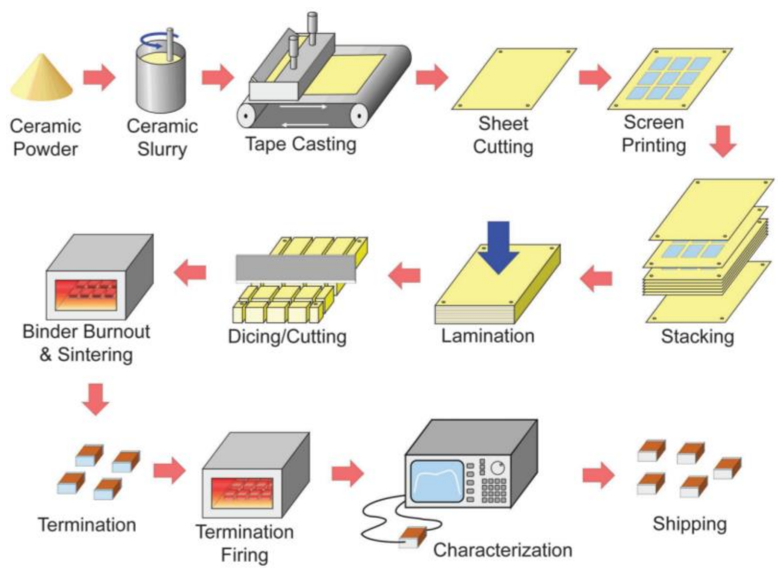

Figure 5 MLCC manufacturing process [3]

1.2 MLCCs as an Alternative to Aluminum Electrolytic Capacitors?

Capacitors are used in a number of applications for the purposes of filtering signals, decoupling, bypass and smoothing. Electrolytic and tantalum capacitors were a capacitors type of choice for filtering purposes due to their high capacitance values [11]. However, problems associated with electrolytic and tantalum capacitors forced design engineers to look for alternatives to be used in filtering applications. Bulky construction, high ESR values, aging in electrolytic capacitors are some the problems in the traditional use of tantalum and electrolytic capacitors [12] [13] [14].

MLCCs on the other hand can turn out to be a viable alternative to electrolytic and tantalum capacitors to be used in filtering applications [15] . MLCCs have smaller case size, large voltage breakdown strengths, and exceptionally high frequency characteristics [16] [17] [18]. Also, MLCCs have low ESR values that results in less heating due to power dissipation when used in ripple current conditions.

1.3 Ripple Current and Self Heating

In DC bias situations, the capacitor charges up to the source voltage after which no current flows through the capacitor other than leakage current (due to imperfections of the dielectric). However, in varying voltage applications, current flows through the capacitor known as ripple current and is given as:

$I = C * dV/dt$, where C is capacitance and dV/dt is the rate of change of voltage.

Figure 6 shows the ripple current caused due to the varying voltage applied on the capacitor. The current flowing through the capacitor causes the temperature of the MLCC to raise due to parasitic resistance associated with the capacitor. Figure 7 shows the real-life capacitor with parasitic resistance and inductance associated with the MLCC. The parasitic resistance is responsible for dissipating power, resulting in self-heating. The power dissipated by the MLCC is given by:

$P = I^2 * ESR$, where I is ripple current and ESR is the equivalent series resistance.

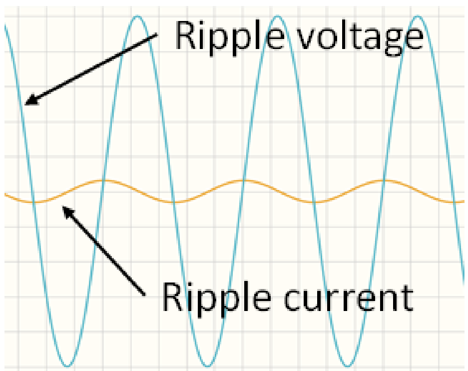

Figure 6 Ripple current due to varying voltage

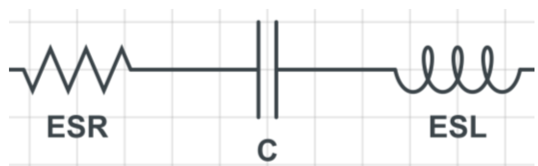

Figure 7 Real capacitor with ESR and ESL

The power dissipated by the parasitic resistance (ESR) of the MLCCs raises its temperature when current flows through it. Operating under elevated temperatures over extended periods of time might degrade the performance of the MLCC resulting in a catastrophic failure or operating outside the limits. The availability of the degradation data or reliability data allows to make better decisions on the choice and the suitability of the MLCC under ripple current conditions. Hence, it becomes necessary to understand the degradation characteristics of the MLCCs before replacing the electrolytic capacitors or tantalum capacitors with MLCCs. Figure 8 shows the surface temperature of the MLCC due to ripple current over a range of frequencies.

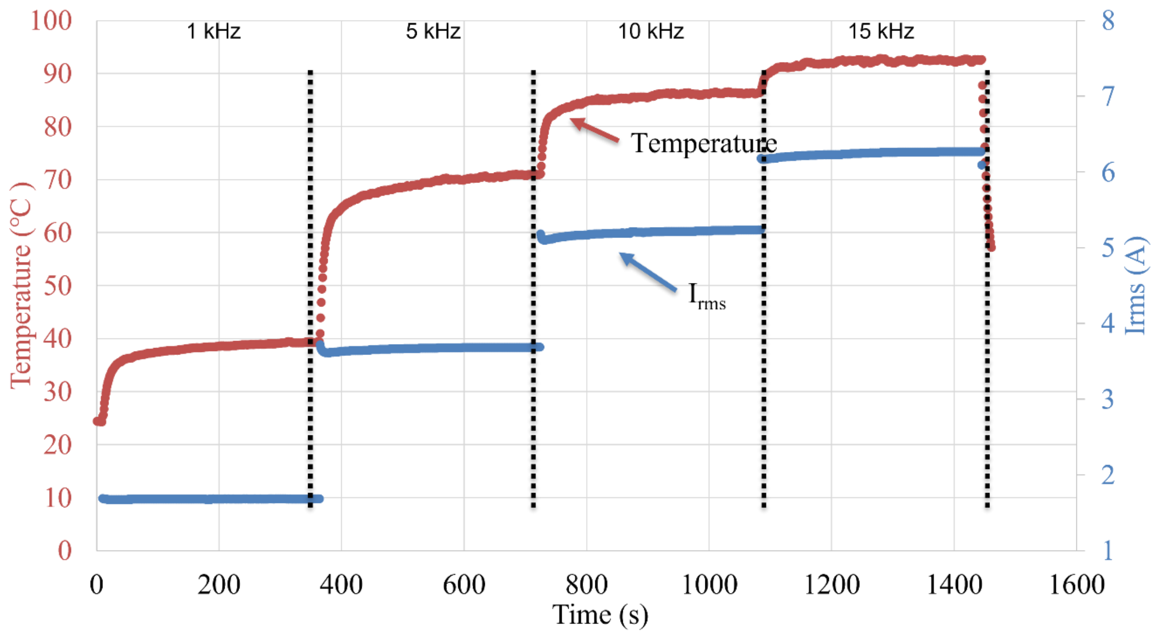

Figure 8 Ripple current and self-heating

1.4 Literature Review

A lot of studies are available on the temperature, humidity, and bias testing on MLCCs. The MLCCs tested degraded in insulation resistance under the application of temperature and DC bias stresses [19] [20] [21] [22] [23] [24]. The widely accepted failure mechanism for the degradation in the insulation resistance is considered to be due to the migration of oxygen vacancies towards the cathode. The oxygen vacancies travel through the grain boundaries while diffusing through them and a few oxygen vacancies get trapped in the grain boundary. The Schottky barrier potential reduces as the oxygen vacancies travel through the grain boundaries and as a result the insulation resistance of the MLCCs decreases eventually leading to thermal runaway [24]. This is the most widely accepted failure mechanism for degradation in insulation resistance of MLCCs tested with temperature and DC bias.

The performance of the MLCCs when used in power pulsation buffers were studied [25]. The capacitance and energy density were reported to change with the applied ripple voltage. The effects of ESR and the volume of the MLCC on the self-heating temperature due to ripple current were studied and recommendations concerning the choice of MLCCs to reduce the internal stress were given [26]. A model to effectively calculate the ESR was also developed for MLCCs operating under combined ripple voltage and DC bias environment [27].

Degradation in the insulation resistance of barium titanate was studied using a range of AC electric fields of 25 kV/cm to 55kV/cm at frequency of 60 Hz and at a temperature of 150℃. At 150℃, barium titanate exists in paraelectric state and does not exhibit piezoelectricity or electrostriction [28]. The effects of AC field on the aging in barium titanate was studied and a drop in the dielectric constant was reported [29].

Manufacturers mention the allowable temperature rise due to self-heating under various ambient conditions but information about the expected failures is not presented. For example, MuRata recommends the maximum temperature rise of 20℃ due to self-heating when operating at a temperature of 25℃.

For applications involving ripple voltage conditions, Class I MLCCs are recommended [30] by manufacturers due to the low ESR, paraelectric dielectric material (which is stable under temperature, time, and DC bias [31]). Class I MLCCs are also robust in the HALT testing as no failures were reported due to oxygen vacancy migration [32] [33]. However, the low volumetric efficiency of the Class I MLCCs and the large case sizes hinder their use in applications involving high ripple voltages and miniaturization.

However, no information about the lifetime and the performance of the MLCCs under ripple current conditions is available. Information about the suitability of MLCCs with various specifications and their degradation characteristics would help the design engineers make better decisions regarding the choice of MLCCs.

1.5 Research Objectives

- To determine the effects of ripple current on the degradation of the multilayer ceramic capacitors
- Determine the failure mechanism leading to the failure of the MLCCs
- Compare between MLCCs of two different voltage ratings to see the effects of voltage ratings on the ripple current performance

2 Ripple Current testing of Multilayer Ceramic Capacitors

To determine the effects of ripple current on the MLCCs, ripple current testing was performed on MLCC samples with two different voltage ratings while keeping the other specifications the same.

2.1 Objectives

- Determine the effects of ripple current of the degradation of the performance of the MLCC
- Determine the failure mechanism in MLCCs subjected to ripple currents
- Determine the effects of voltage ratings on the performance of MLCCs

2.2 Approach

- MLCCs with two different voltage ratings were selected for the testing while keeping the manufacturer and the other specifications the same. The details of the MLCCs selected are mentioned in Table 1
- The MLCCs were de-aged by placing them inside the oven at 150℃ for 30 minutes to reset the capacitance and to ensure a common starting point for all the MLCCs
- Capacitance, dissipation factor and insulation resistance were measured at several points, including before after the soldering, de-aging and before

starting the experiment and at predetermined intervals during the experiment

- Ripple current testing was performed on the MLCCs by applying temperature and ripple voltage stresses
- Capacitance, dissipation factor and insulation resistance readings were measured at regular intervals after cooling the samples to room temperature
- After failure, the samples were inspected for physical defects using optical microscopy
- Thermally stimulated depolarization study was then carried out to observe the relaxation of defects in the bulk of the dielectric material

2.3 Ripple Current Testing of Multilayer Ceramic Capacitors

Four MLCC samples from each voltage ratings were tested for ripple currents. Two controls were used at room temperature and other two control were used as control at 85°C inside the oven. The purpose of the controls was to detect any changes in the measurement system. Class II X7R dielectric MLCCs were used for the testing. The specifications can be found in the Table 1. The ripple current test conditions used in the testing can be found in Table 2. Controls at room temperature were used to observe any drift in the measurement instruments and controls at 85°C were used in order to observe the effects of temperature on the performance of the MLCCs.

	A	B
Capacitance	1µF	1µF
Voltage rating	6.3 V	16 V
Case size	1206	1206
Dielectric	X7R	X7R
Manufacturer	Kemet	Kemet
Dielectric material	Barium titanate	Barium titanate
Rated temperature	-55 to 125℃	-55 to 125℃

Table 1 Specifications of the MLCCs used in ripple current testing

	6.3 V MLCCs	16 V MLCCs
Applied AC voltage (0 to peak)	12.6 V	12.6 V
Frequency	25 kHz	25 kHz
Ambient temperature	85	85
Ripple Current samples	4	4
Controls (Room temperature)	2	2
Controls (85℃)	2	2

Table 2 Life test plan

Ripple current causes self-heating, resulting in the temperature of the MLCC to rise. The amount of power dissipated, and the temperature rise of the MLCCs depends on the ESR (equivalent series resistance) and the thermal resistance offered by the MLCCs. The surface temperature of the MLCC, due to a combination of ambient temperature and self-heating due to ripple current, was limited to a maximum of 115°C in order to prevent the phase transition of barium titanate from ferroelectric to paraelectric. The phase transition of barium titanate from ferroelectric to paraelectric phase occurs above the Curie temperature (130°C). In the paraelectric phase, barium titanate loses it piezoelectric properties . In order to retain the piezoelectric properties of barium titanate, the surface temperature was limited to a maximum of 115°C.

The electrical parameters of the MLCCs, like capacitance, dissipation factor and insulation resistance, were measured before and after the testing and also at regular intervals during the ripple current testing. The parameters were measured once every day at room temperature for the first 855 hours of testing, followed by measuring the parameters once every two days for the next 1145 hours of testing. The failure criteria for capacitance measurement were set to 10% drop from the rated capacitance, increase in ESR above 5% and fall in insulation resistance below 500 ΩM. Testing was continued on all the samples till the 2000 hours were completed. Failure analysis was then performed on the samples that degraded in insulation resistance using both nondestructive and destructive physical analysis.

2.4 Instruments Used and Measurement Conditions

Figure 9 shows the complete test setup used for performing ripple current testing. The MLCCs parameters were measured at room temperature. All the MLCC samples were connected to the measurement instruments through the multiplexer switch unit (Agilent 34980). The multiplexer switch unit directs the signals from the measurement instruments to the sample of interest. Short and open correction is performed before every measurement cycle on the LCR meter. All the MLCCs were discharged for five minutes through a discharge capacitor before every measurement cycle. A 1 kΩ resistor was connected in series with the high resistance meter to prevent the surge current from damaging the ammeter.

Name	Function	Condition
Agilent E4980A	To measure the capacitance and dissipation factor	At 1 V_{rms} at 1 kHz (Manufacturer recommended)
Agilent B2985	To measure the insulation resistance	At the rated voltage for 2 minutes (Manufacturer recommended)

Table 3 List of instruments used

The measurement and the testing were automated with the help of a LabView program. The LabView code was responsible to initiate the measurement sequence after a set ripple time and also to monitor the current in real time to proactively stop the testing in case of short circuit. Figure 10 shows the soldered MLCC samples connected to the ripple voltage source and to the multiplexer unit.

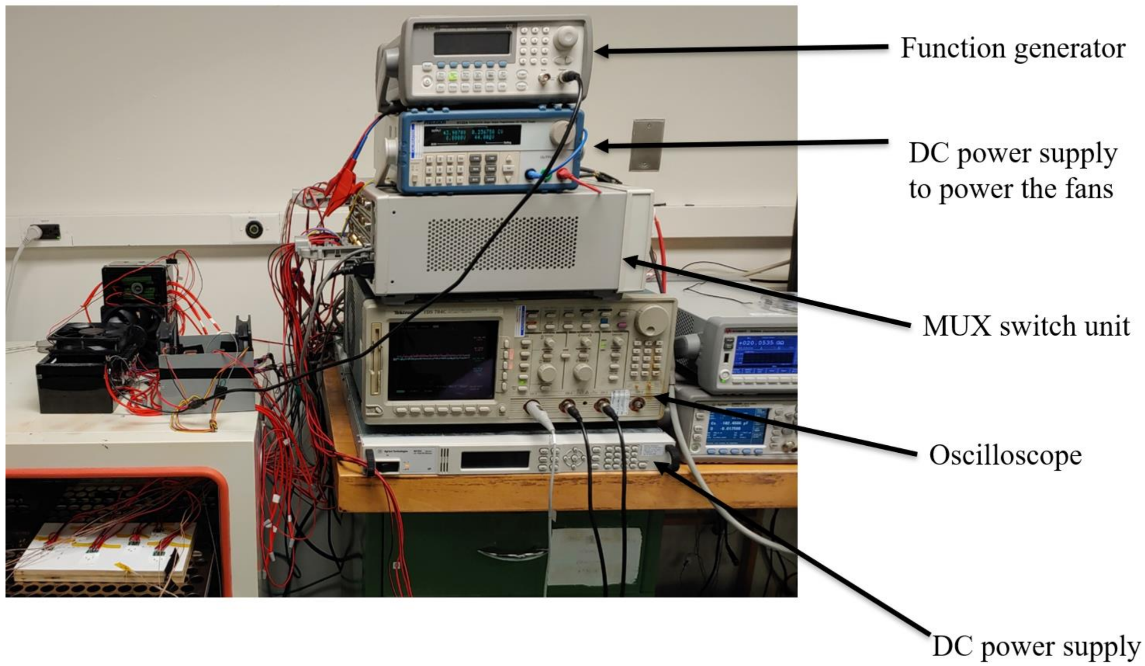

Figure 9 Ripple current setup

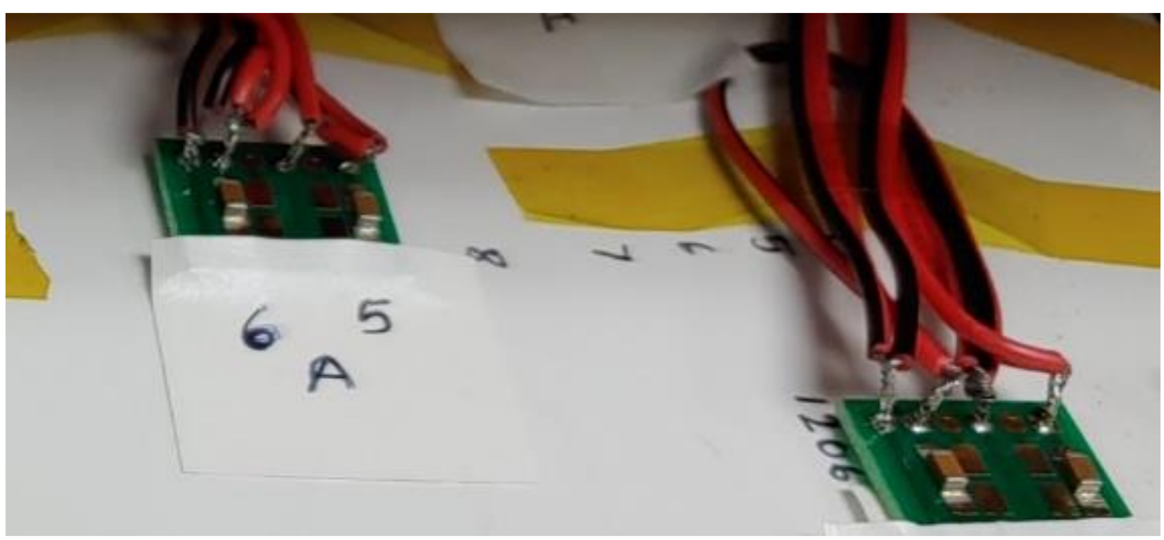

Figure 10 Test MLCCs soldered on SMD boards

2.5 Ripple Current Test Results

The current flowing through the capacitors was measured to be 1.9 A_{rms}. The temperature of the MLCC increased to 115℃ from an ambient temperature of 85℃ due to the power dissipated. The MLCC used in the test was rated for a maximum operating temperature of 125℃, however, temperature of the MLCCs in the ripple current testing was limited to a maximum of 115℃ to prevent the phase transition of barium titanate. order to retain the piezoelectric properties of the MLCCs . Over the Curie temperature (120-130℃), barium titanate exists in cubic phase and exhibits paraelectric properties, whereas below the Curie temperature, barium titanate exists in tetragonal phase and exhibits ferroelectric properties [34] [35]. All ferroelectric materials are piezoelectric in nature, and they exhibit electrostrictive response when an external field is applied. The electrostrictive response exhibited by barium titanate might causing cracking when an AC field is applied. In order to retain the piezoelectric response, the surface temperature of the MLCCs was limited to 115℃.

Figure 11 and Figure 12 show the capacitance plot of the individual MLCCs under ripple current tests. From the data collected over the 2000 hours, the capacitance off all the MLCCs was within the manufacturer's specifications. Figure 13 and Figure 14 show the normalized capacitance plot that is normalized to readings at time 0. Capacitors C1 and C2 are controls at room temperature; C3, C4, C5, C6 are ripple current samples and C7, C8 are controls at 85℃.

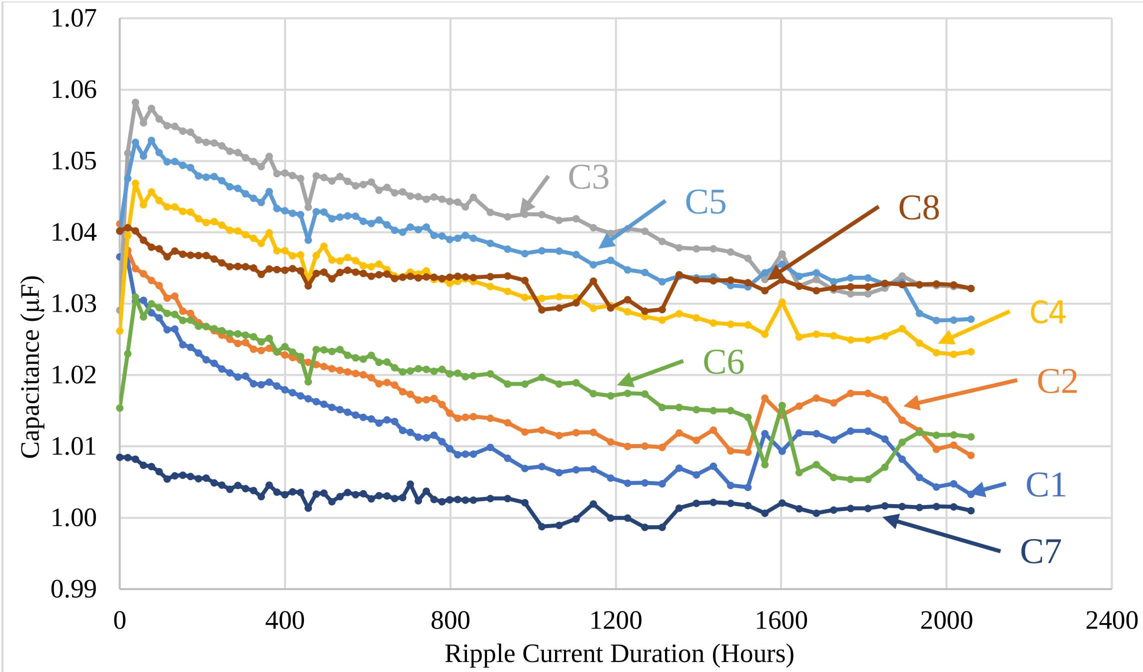

Figure 11 Capacitance plot for 6.3 V MLCCs

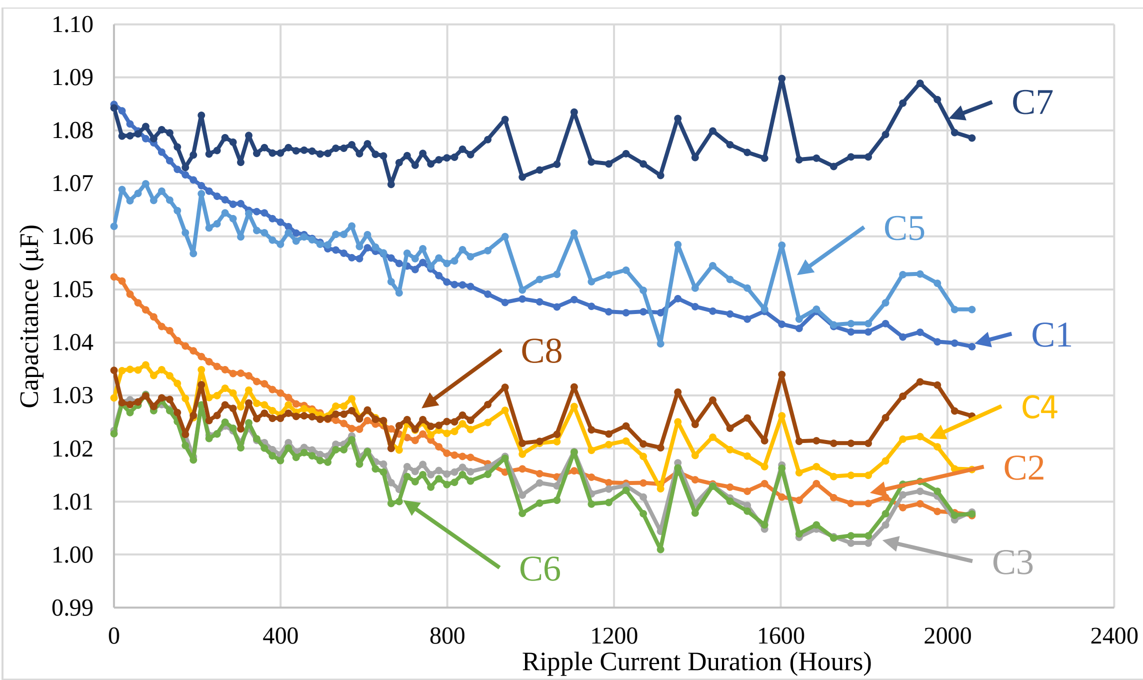

Figure 12 Capacitance plot for 16 V MLCCs

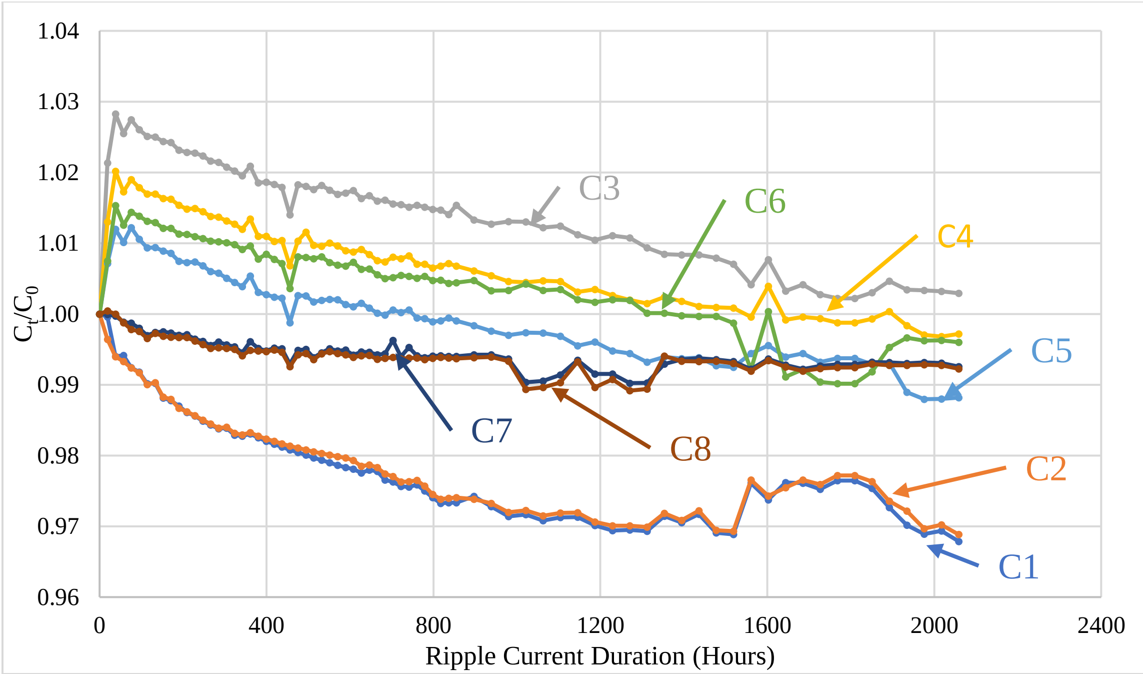

Figure 13 Normalized capacitance values for 6.3 V rated MLCCs

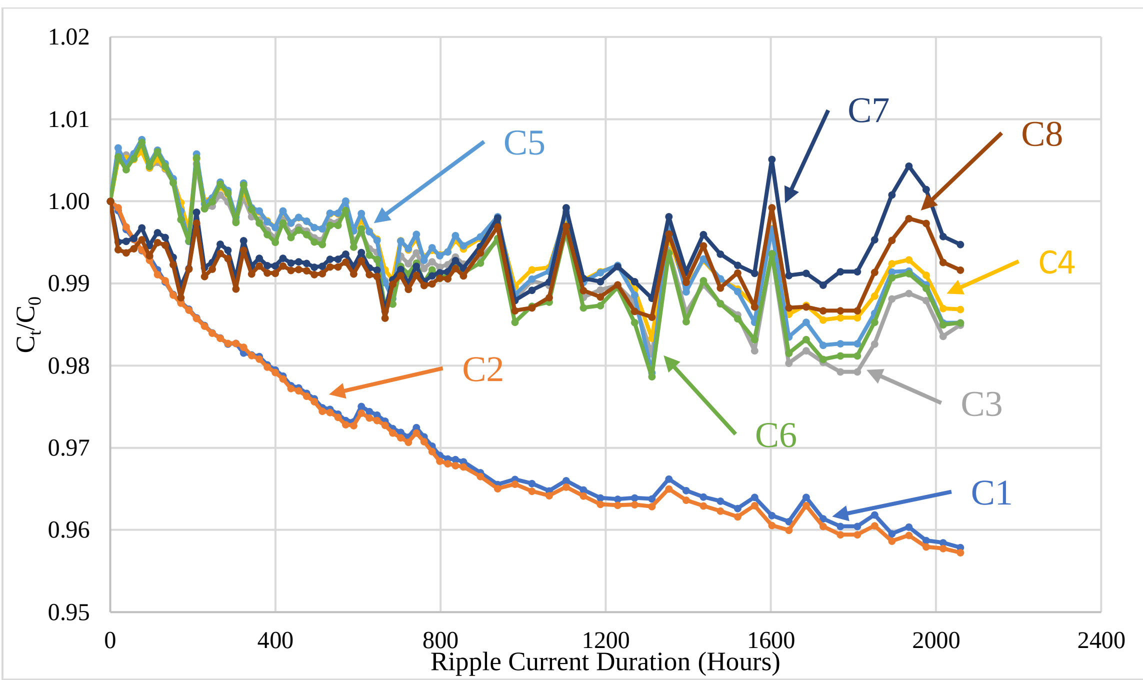

Figure 14 Normalized capacitance values for 16 V rated MLCCs

For the controls at room temperature, a downward trend can be seen in the capacitance that can be attributed to the aging phenomenon associated with class II MLCCs [36]. Class II MLCCs are made with ferroelectric dielectric material that ages overtime. Below the Curie temperature, barium titanate exists in tetragonal phase and over the Curie temperature, the barium titanate exists in cubic structure. When the MLCCs are heated to over the Curie temperature (130°C) and allowed to cool, the barium titanate changes from cubic phase to tetragonal phase. Figure 15 shows the different phases of barium titanate at different temperatures.

In the tetragonal phase, the barium titanate forms dipoles, due to elongation of titanium ion along its axis. which results in spontaneous polarization. The bulk of the barium titanate consists of randomly oriented domains, with the dipoles oriented along the same direction in each domain. This spontaneous polarization gives class II MLCCs high capacitance values.

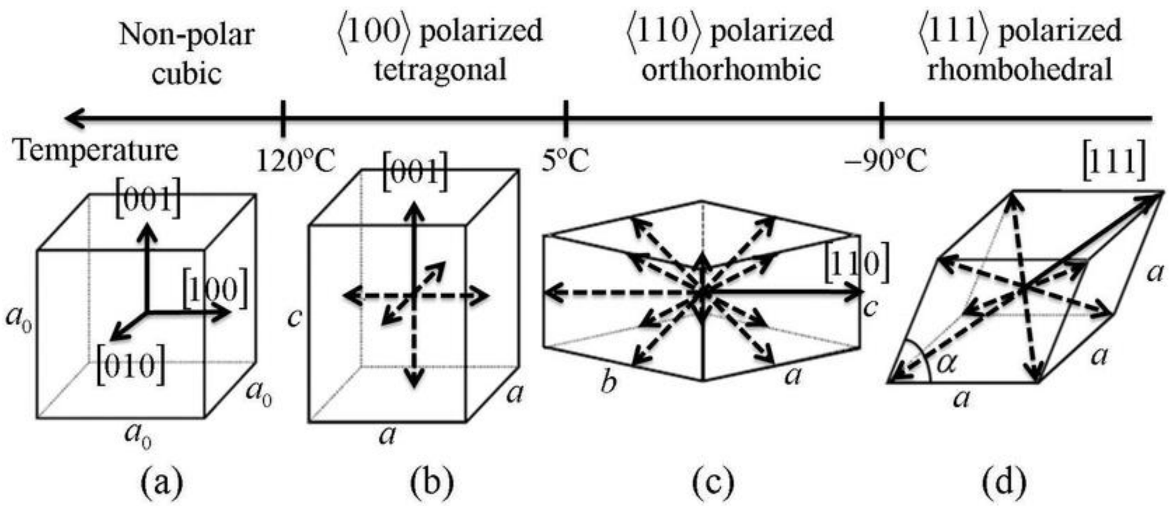

Figure 15 Various phases of barium titanate [37]

However, the dipoles that were randomly distributed, align themselves in a stable energy state thereby reducing the dielectric constant of barium titanate throughout the life of the MLCC [38] [39] [40] [41]. The drop in the dielectric constant results in the drop in the capacitance and this drop occurs in a logarithmic fashion [39]. The phenomena of drop in capacitance of class II are referred to as aging. Figure 16 shows the changes in the orientation of domains from randomly organized to reorienting themselves into a much more stable fashion. The process of aging is not a permanent, and it can be reversed by baking the MLCCs over the Curie temperature for some time. Manufacturers recommend the baking conditions of 150℃ and for a duration of 30 minutes.

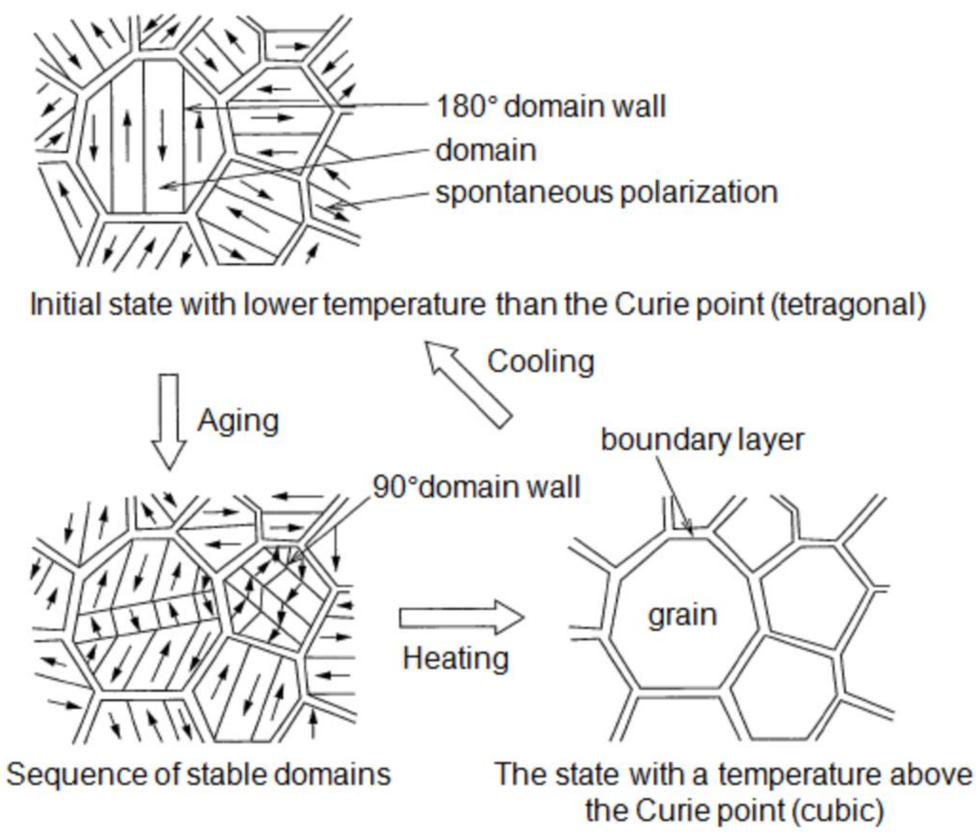

Figure 16 Dipole relaxation on cooling leading to aging [42]

Aging rates for the class II X7R MLCCs vary from 2% to 7% per decade hour and it can be found from the manufacturer specification sheet. Figure 17 shows the typical aging behavior of a class II X7R MLCC having a nominal capacitance of 1μF. The capacitance at any point time after baking it to over the Curie temperature can be calculated using the aging equation as mentioned below.

$$C_t = C_{ref} *(1 + (\text{Aging Rate}) * (\text{Log} (\text{Referee Time (H)}) - \text{Log} (\text{Test Time (H)}))$$

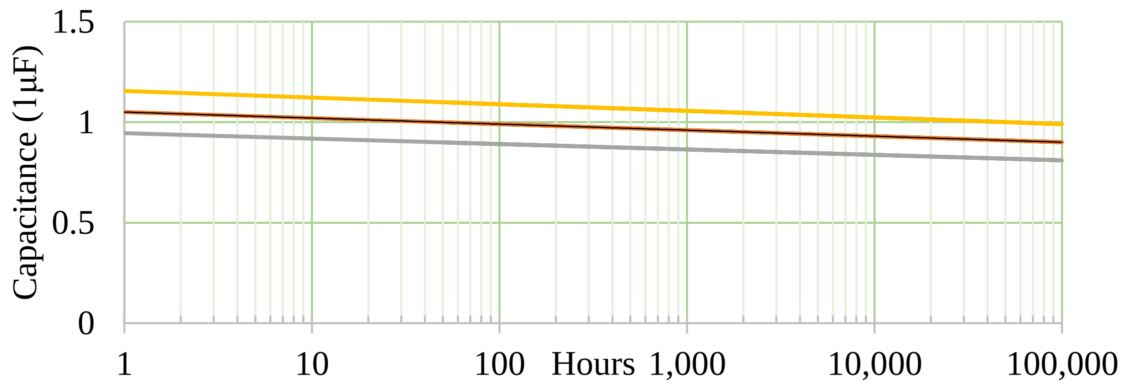

Figure 17 Aging in class II X7R MLCCs

Aging can also be observed in the ripple current samples. Aging in the ripple current samples can be explained with the help of the hysteretic domain wall motion that is driven by the applied electric field. The effects of domain wall motion under the influence of externally applied electric field was studied and reported [29].

Figure 18 and Figure 19 shows the dissipation factor plot for 6.3 and 16 V rated MLCCs. The limit for the dissipation factor as set by the manufacturer was 5%. After 2000 hours of ripple current testing, it was observed that the dissipation factor of all the samples is well below the manufacturer's specifications.

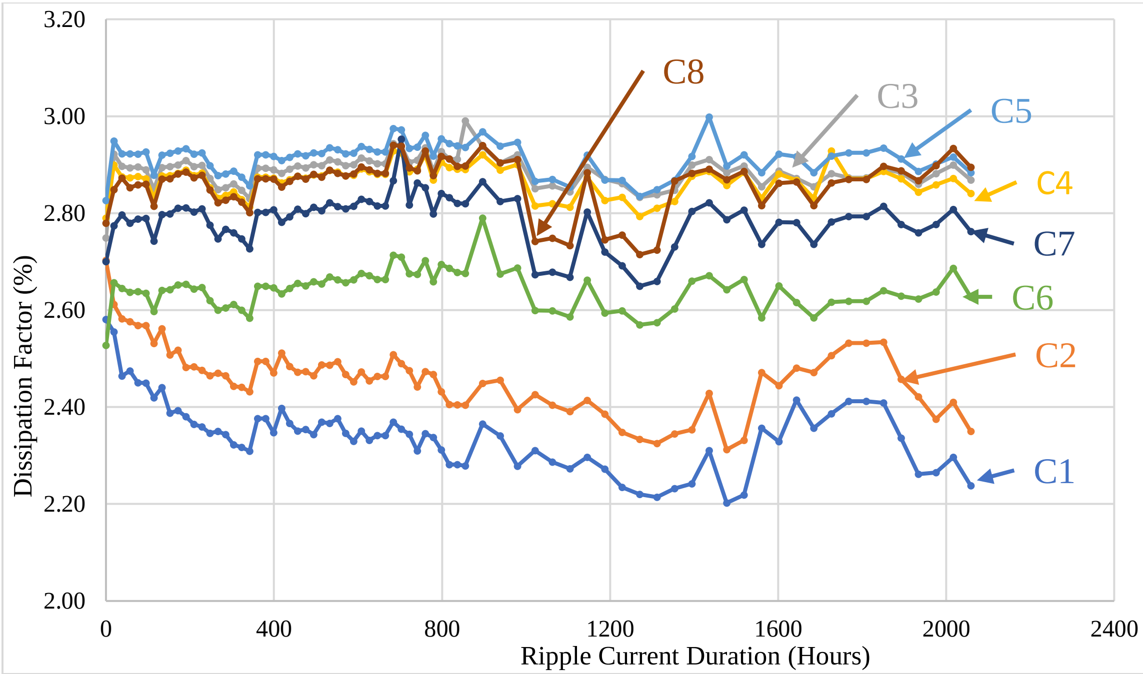

Figure 18 Dissipation factor plot for 6.3 V MLCCs

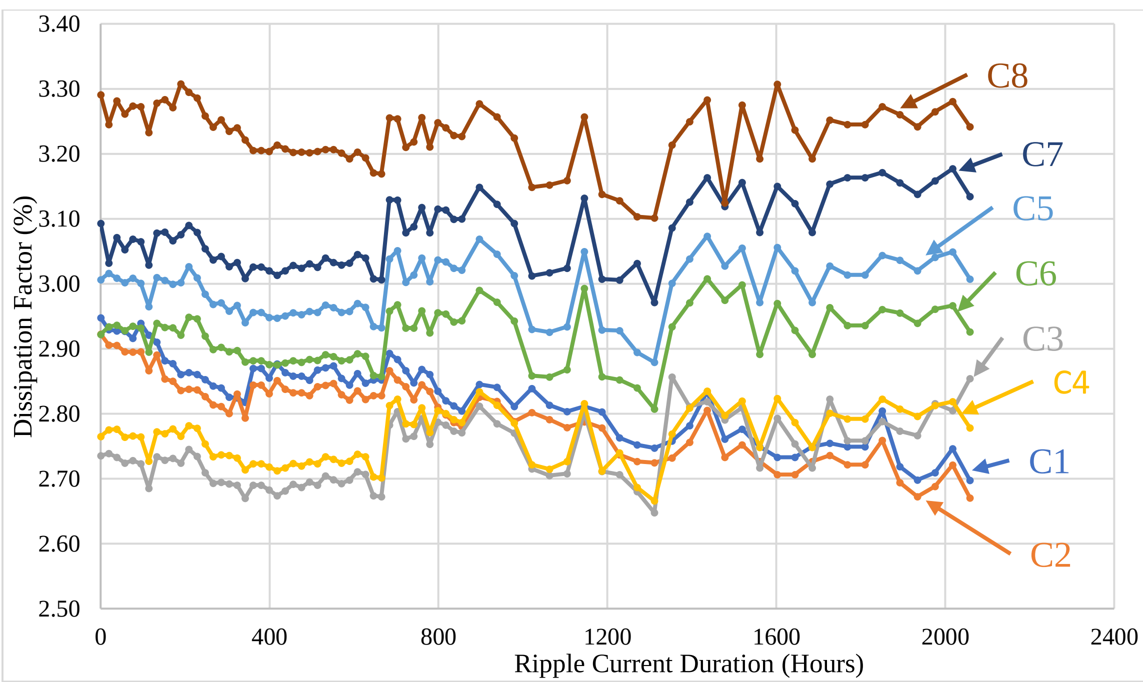

Figure 19 Dissipation factor plot for 16 V MLCCs

Figure 20 shows the insulation resistance plots for individual MLCCs. Degradation of insulation resistance of the MLCCs rated for both the 6.3 V and 16 V rated MLCCs can be seen. Three out of four MLCCs tested from each voltage rating degraded below their initial values. One of the 6.3 V rated MLCCs dropped in insulation resistance from an initial value of 17 GΩ to around 200 MΩ, falling below the lower limit as defined by the manufacturer specification of 500 MΩ. The other two capacitors from the same voltage specification too showed degradation in the insulation resistance, however they were over the manufacturer specification.

Figure 21 shows the insulation resistance of the 16 V rated MLCCs. It can be observed that the 16 V rated MLCCs too showed significant degradation in the insulation resistance in spite of operating at a derated condition (working at 80% of their rated voltage). One of the MLCCs dropped in insulation resistance below the manufacturer specified lower limit of 500 MΩ. The other two capacitors degraded in the insulation resistance; however, they were over the manufacturer specification. The possible failure mechanism and additional analysis performed on the MLCCs will be discussed in the next chapter.

Operating the 16 V rated MLCCs at a derated voltage showed no significant improvement in the degradation of the insulation resistance in comparison to the 6.3 V rated MLCC that was operated at twice its rated voltage. This raises the question about the effectiveness of derating the MLCCs with respect to the voltage ratings assigned by the manufacturer.

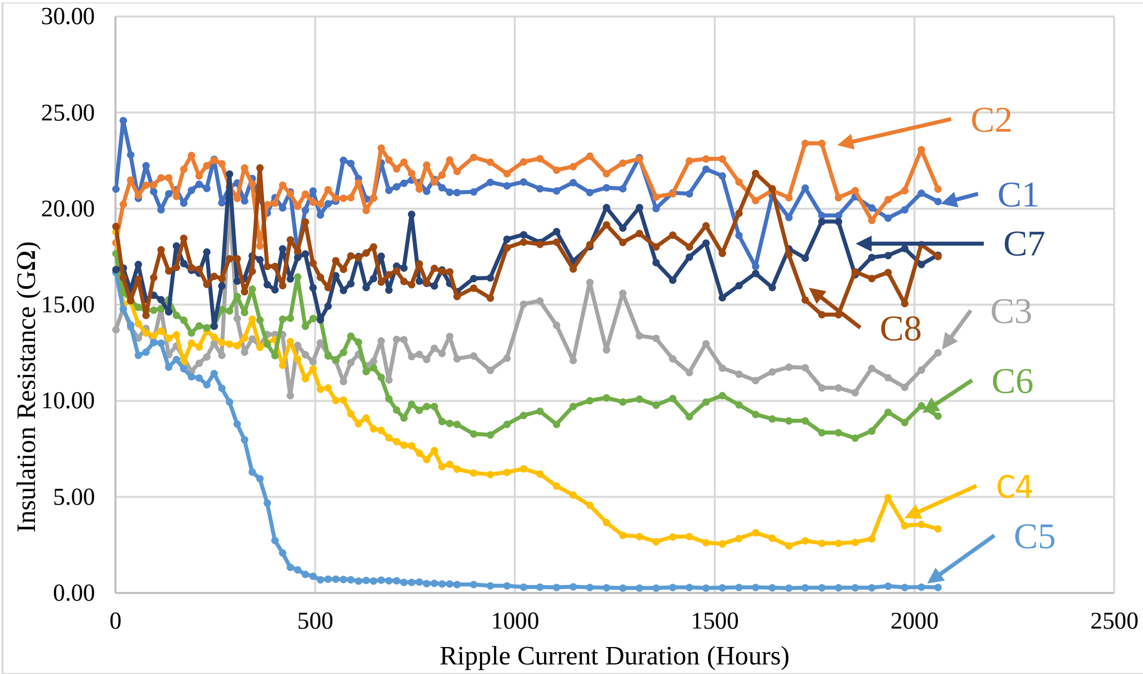

Figure 20 Insulation resistance plot for 6.3 V MLCCs

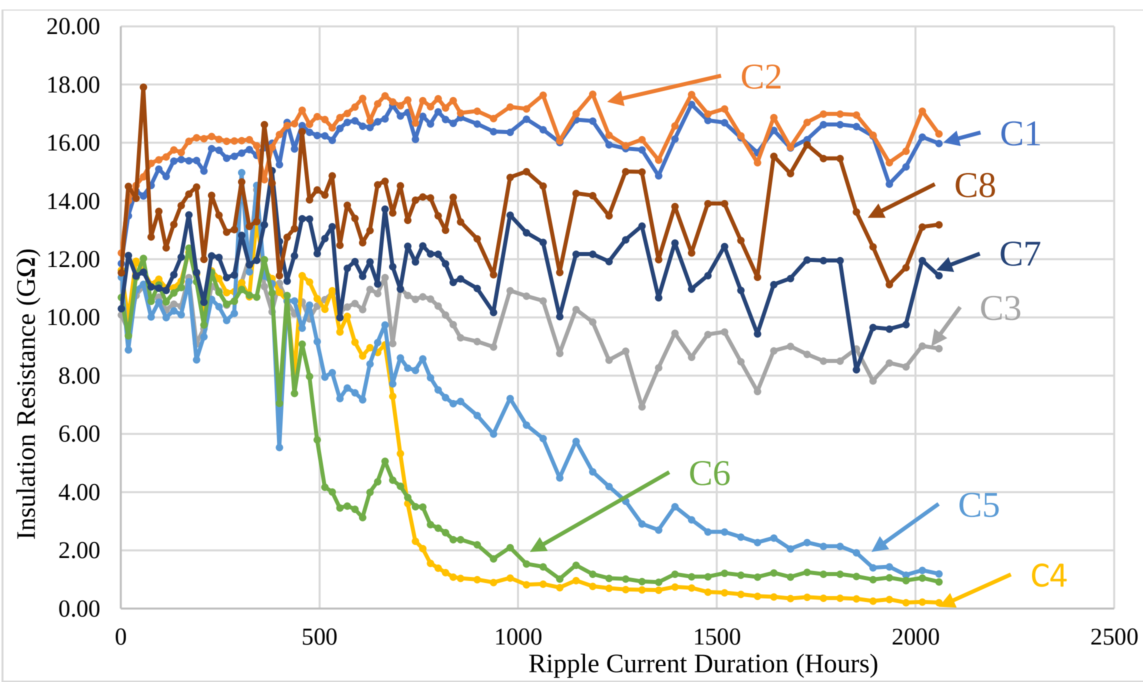

Figure 21 Insulation resistance plot for 16 V MLCCs

To check for the consistency and for the repeatability of the tests, the ripple current testing was conducted on other MLCC samples with different specification from the same manufacturer. The trends in drop in the capacitance of the samples can be seen. Also, similar toe the test results shown above, the degradation in the insulation resistance can be seen in the following ripple current tests. Table 4 shows the specifications of the samples used for the tests. Figure 22 and Figure 23 are the capacitance plots for the samples. Figure 24 and Figure 25 are the dissipation factor plots, and Figure 26 and Figure 27 are the insulation resistance plots for the samples being tested.

Table 4 Ripple current sample specifications

	A	B
Capacitance	1μF	1μF
Voltage rating	6.3 V	6.3 V
Case size	0805	0603
Dielectric	X7R	X7R
Manufacturer	Kemet	Kemet
Dielectric material	Barium titanate	Barium titanate
Rated temperature	-55 to 125℃	-55 to 125℃

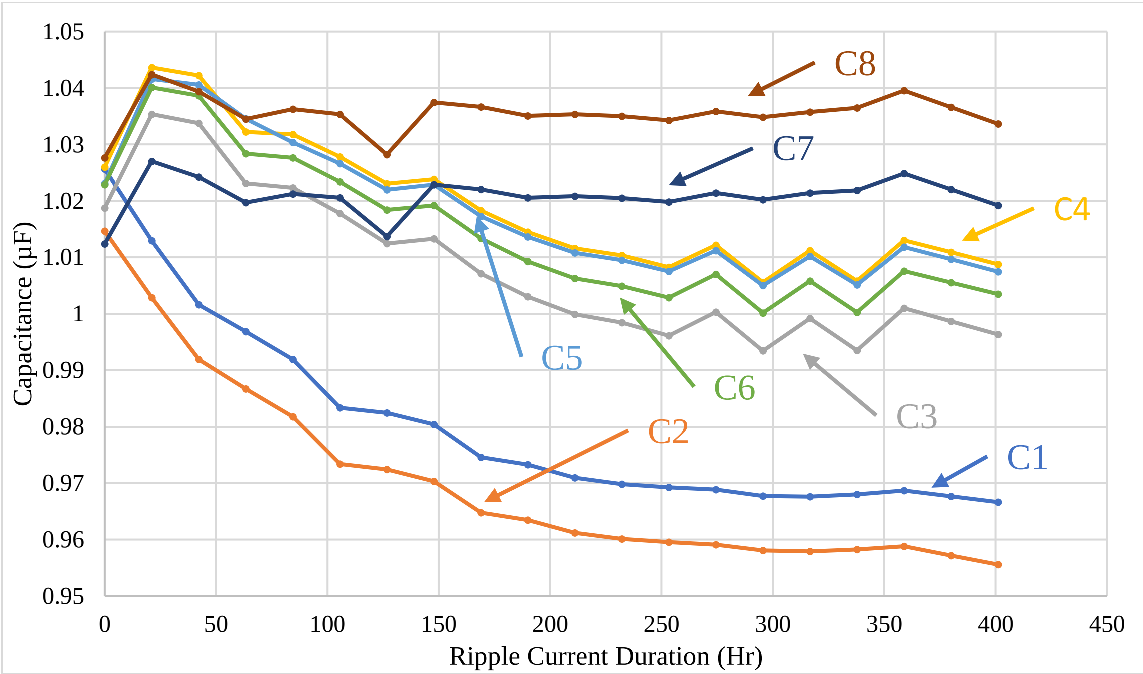

Figure 22 Capacitance plot for 0805 MLCC

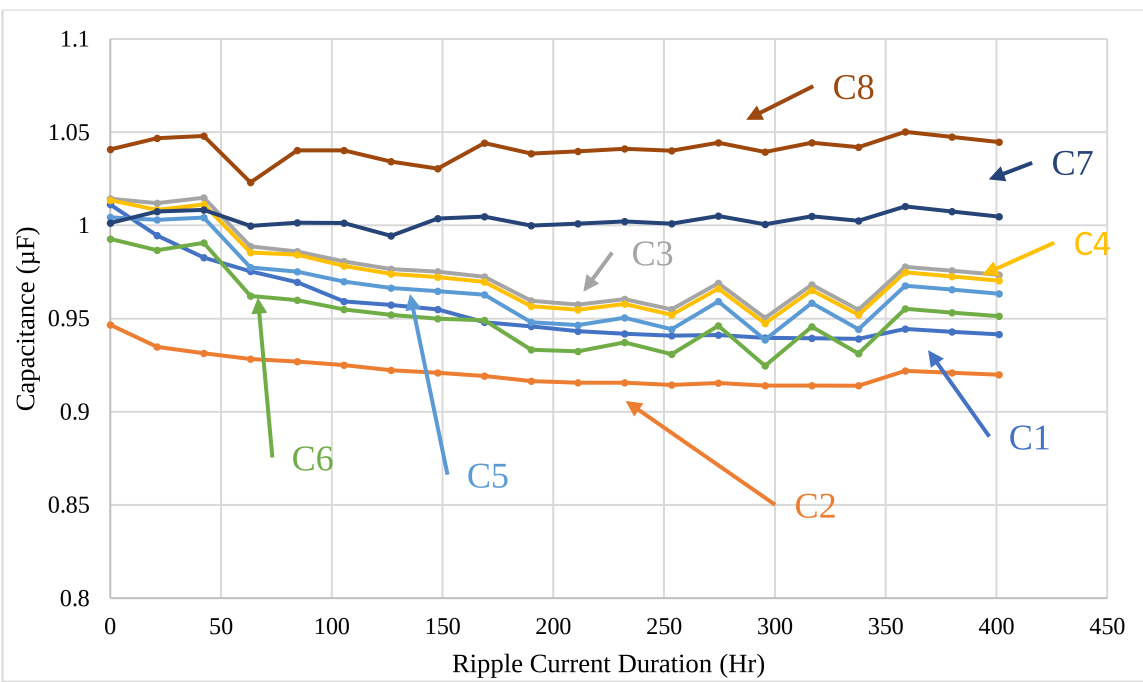

Figure 23 Capacitance plot for 0603 MLCC

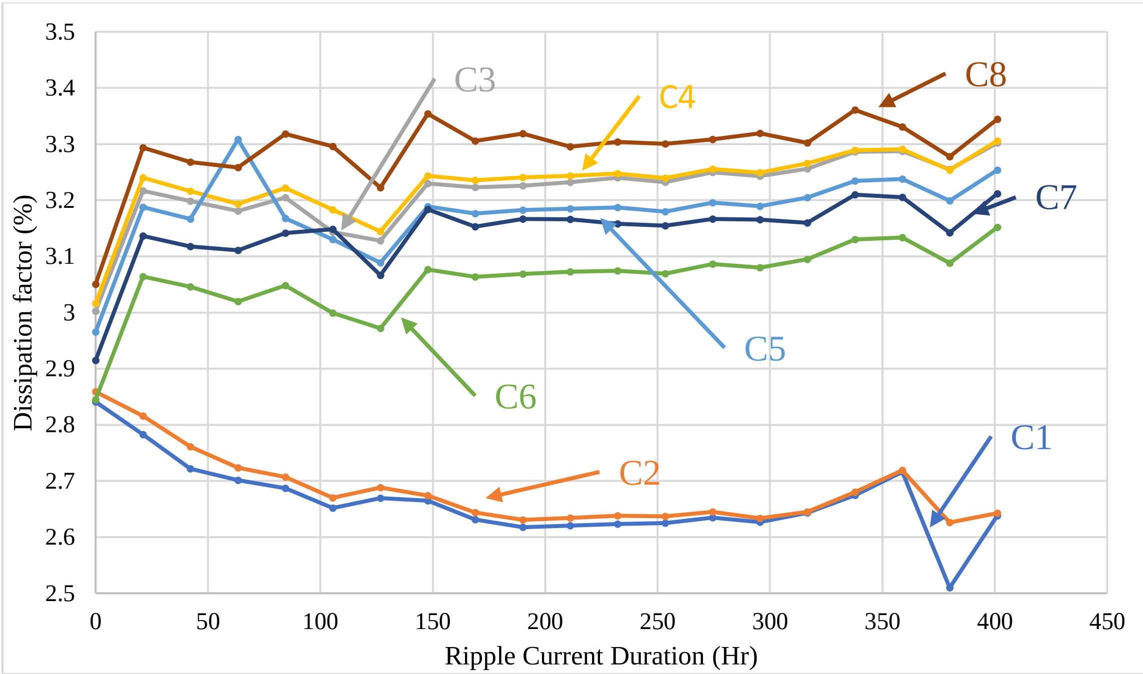

Figure 24 Dissipation factor plot for 0805 MLCC

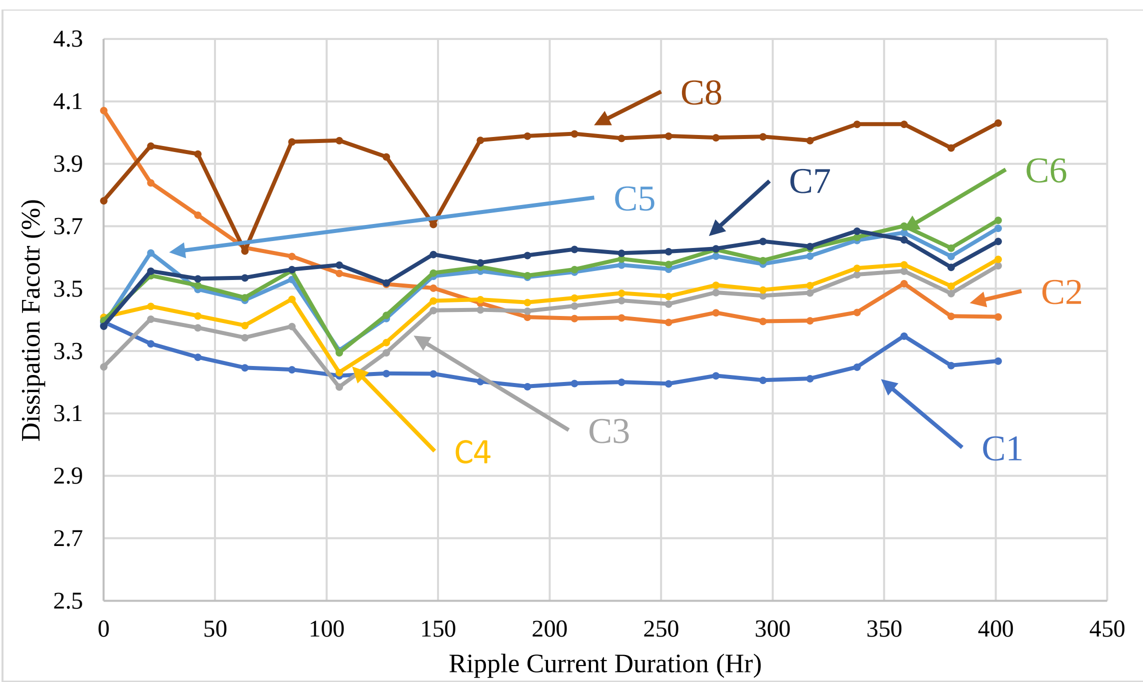

Figure 25 Dissipation factor plot for 0603MLCC

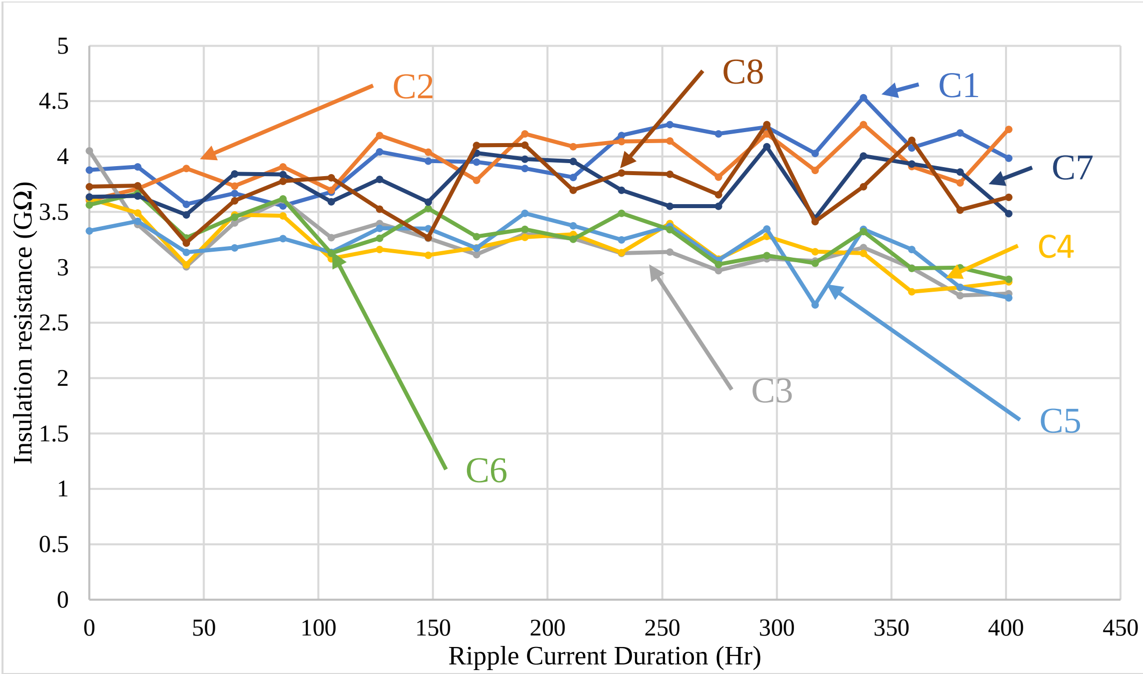

Figure 26 Insulation resistance plot for 0805 MLCC

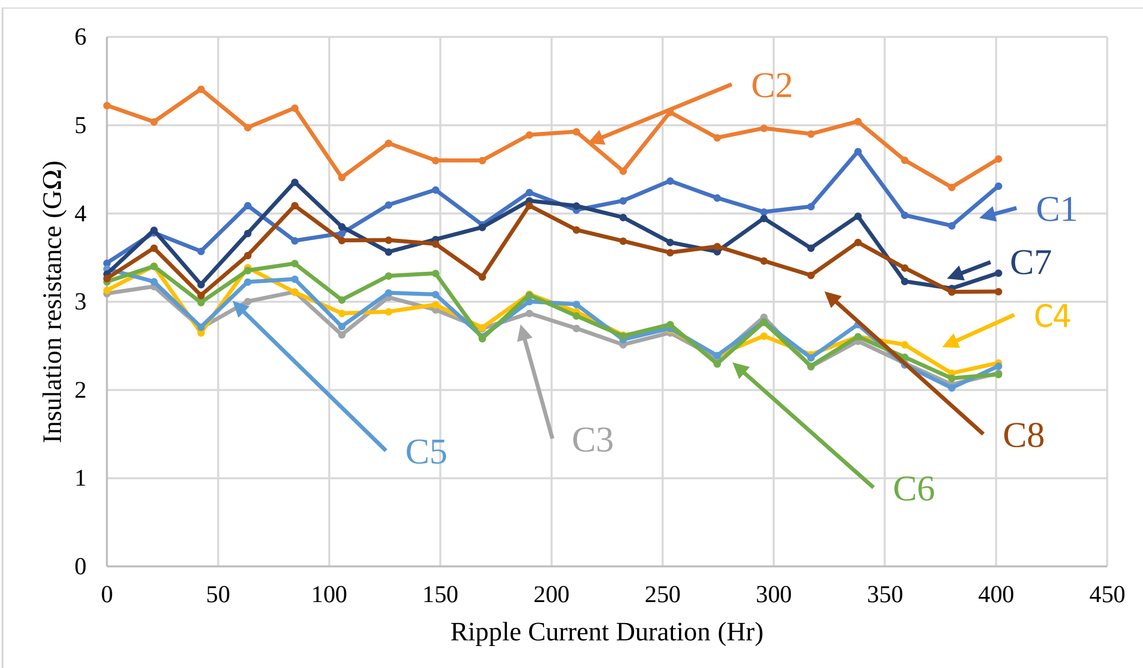

Figure 27 Insulation resistance plot for 0603 MLCC

In summary:

- Ripple current testing was performed on MLCCs with two different voltage ratings
- The capacitance and the dissipation factor of all the samples remained within the manufacturer specifications
- The capacitance of the room temperature controls was decreasing due to well-known phenomenon associated with class II X7R MLCCs called as aging
- The drop in the capacitance of the ripple current samples can be due to the domain wall motion due to the application of an external electric field
- The insulation resistance of the ripple current samples degraded

3 Failure Analysis of Degraded Samples

Degradation in the insulation resistance of dielectrics is a common problem related to capacitors. Insulation resistance degradation due to oxygen vacancy migration is the most common type of degradation mechanism in barium titanate under the application of temperature and DC bias [24]. Cracking in MLCCs is another reason for the degradation in the insulation resistance.

3.1 Insulation Resistance Degradation Due to Cracks

MLCCs are very brittle in nature and can crack easily while in the assembly process. Board flexing, bad soldering practices are some of the common causes for cracks in MLCCs during the assembly process [43] [44].

Apart from the assembly process, cracks can occur in the MLCCs while operating in a variety of conditions. The dielectric material used in class II X7R MLCCs is barium titanate, which is a ferroelectric material. All ferroelectric materials exhibit piezoelectricity, and in the presence of an electric field, the MLCCs undergo compression or elongation depending on the direction of the electric field applied. Figure 28 demonstrates the piezoelectric effects. The rapid deformation of the MLCC caused due to charging and discharging currents flowing through it can cause cracks. Severe cracking in the MLCCs were reported while operating at the piezoelectric resonant frequency of the MLCC [45] [46]. Cracks can also occur due to the formation of a thermal gradient as a result of current flowing through the capacitor [46].

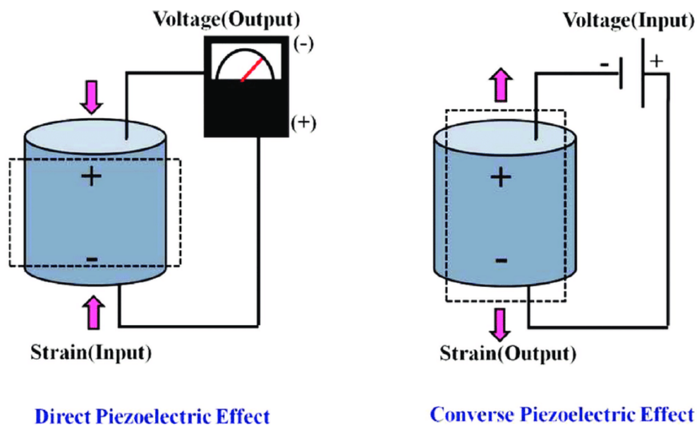

Figure 28 Electrostriction in MLCCs [47]

Figure 29 Cracked MLCC operating at its piezoelectric resonant frequency [45]

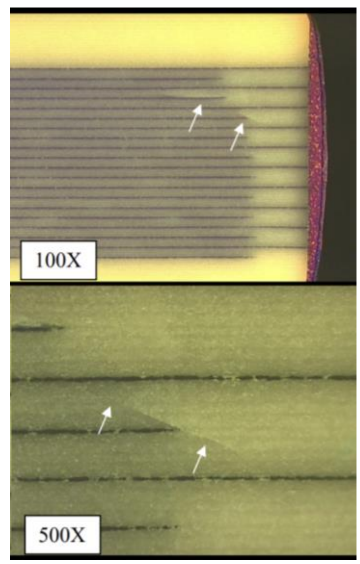

Figure 30 Cracked MLCC under surge current conditions [46]

Formation of cracks can severely affect the lifetime of the MLCCs. A crack connecting two active electrodes can result in lowered insulation resistance and at times a short connection. If the applied voltage exceeds the breakdown voltage of the air filled in the cracks, a sudden discharge takes place degrading the dielectric material.

Alternatively, in a humid environment, moisture can enter the crack in the dielectric material. A short connection will be formed if the cracks occur in the active region of the electrodes . The low resistance path formed causes current to flow through the crack resulting in the degradation of the dielectric [43] [48] [49]. Figure 29 shows a crack formed in the MLCC as a result of operating at its piezoelectric resonant frequency. Figure 30 shows a crack in the MLCC due to the passage of repeated cycles of surge current through the MLCC.

3.2 Degradation Due to Oxygen Vacancy Migration

The oxygen vacancies appear in the bulk of the barium titanate during the sintering process. In class II MLCCs, the electrode is made of nickel and with the ceramic as barium titanate. During the manufacturing process, to prevent the oxidation of nickel electrodes, the sintering of the MLCCs is done in reducing atmospheres and at a temperature of around 1100°C. While sintering, the oxygen present in the barium titanate is used up leaving behind the oxygen vacancies in the bulk of the dielectric material . As the oxygen from the dielectric is used up, it creates positively charged oxygen vacancies within the bulk of the dielectric material [50]. Attempts to reduce the number of oxygen vacancies by re-oxidizing the barium titanate does not remove all the oxygen vacancies and there are still high chances of the presence of oxygen vacancies. Figure 31 shows several processes involved in the manufacture of MLCCs and Figure 32 shows the oxygen vacancies in the bulk of barium titanate after the sintering process.

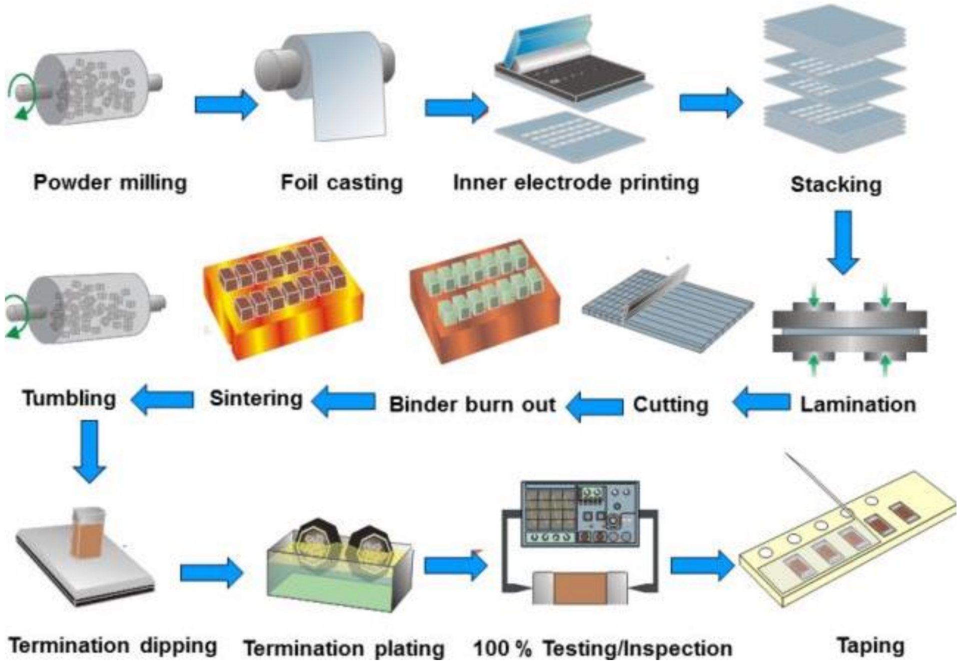

Figure 31 Manufacturing of MLCCs [51]

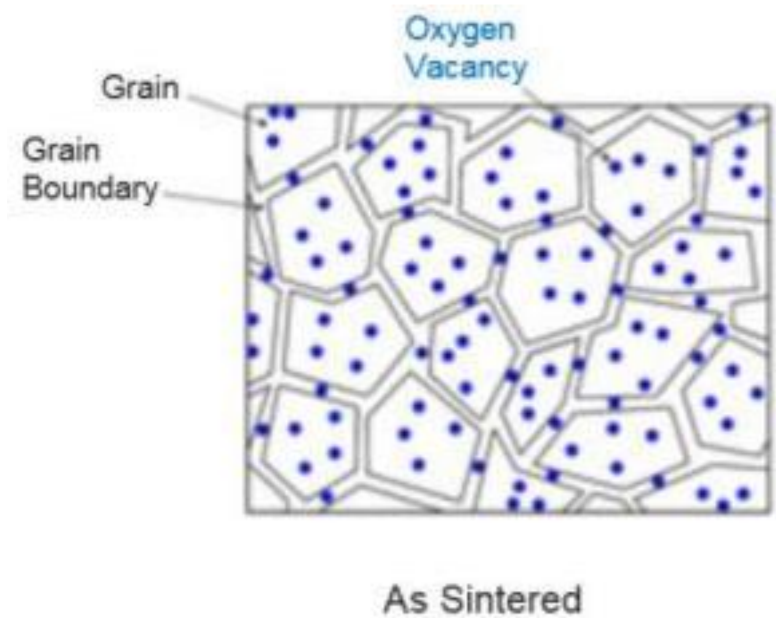

Figure 32 Oxygen vacancies in the dielectric [51]

A lot of information is available on the degradation of insulation resistance in class II X7R MLCCs subjected to temperature and DC bias testing. Test procedure and results of from some previous studies are mentioned. HALT was conducted on in house produced MLCCs at 140°C under 400 VDC field. The testing was stopped when the insulation resistance of the samples dropped lower than 90% of its initial value. Failure analysis was conducted on the degraded samples and the resistance of each of the elements, electrode dielectric interface, grain boundaries, bulk of barium titanate, was studied. Accumulation and clustering of oxygen vacancies was observed in the degraded samples that was not present in the as produced capacitors. The grain boundaries act as barrier to the electromigration of defects resulting in the accumulation of oxygen vacancies at the grain boundaries. In an as produced capacitor, the Schottky barrier was reported to be symmetrical across the grain boundary, but in the DC degraded sample, asymmetry was created due to the accumulation of oxygen vacancies on one side of the grain boundary. Due to the asymmetry, the Schottky barrier is lower on one side of the grain boundary than the other side. This reduced the activation energy of the grain boundary thereby increasing the conductivity. Also, it was reported that the oxygen vacancies pile up at the dielectric and electrode interface increasing the donor content and reducing the resistance near the interface [19]. Figure 33 shows the electromigration and accumulation of oxygen vacancies towards the cathode leading to the drop in insulation resistance.

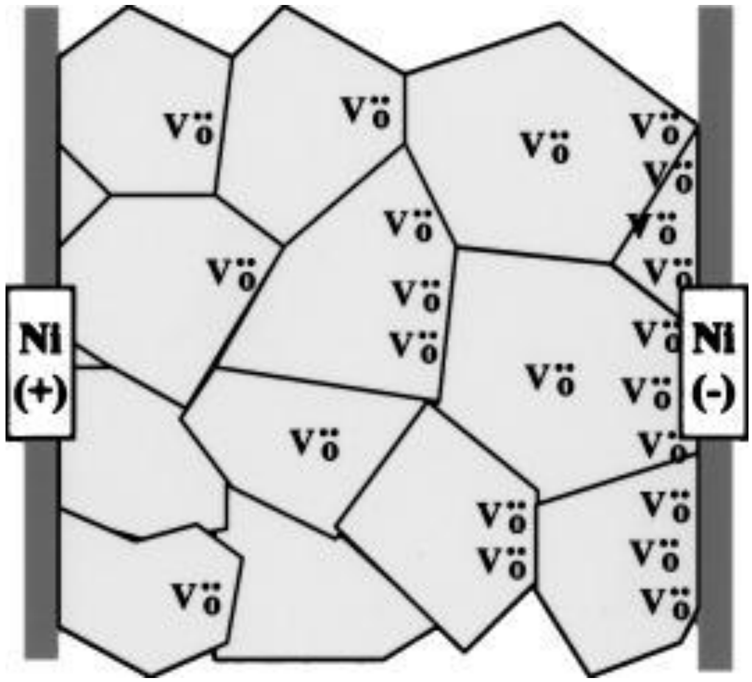

Figure 33 Electromigration of oxygen vacancies towards the cathode [51]

In another study, HALT was conducted on class II X7R MLCCs from three different manufacturers with the following specifications- case size: 0805, voltage ratings: 50 V, capacitance: 0.47μF. Several combinations of stress levels of temperature and voltage were used to test the MLCCs, and the testing was stopped when the leakage current of the MLCCs exceeded 100 μA. The failure mechanism proposed by the authors goes hand in hand with the one explained above. The oxygen vacancies travel towards the cathode under the influence of an external applied DC field. Some oxygen vacancies get trapped near the grain boundary whereas majority of the oxygen vacancies travel continuously towards and accumulate at the dielectric cathode interface creating a net positive charge. To compensate for the build of the positive charge, electrons from the cathode localize at the interface. Overtime, the accumulation of oxygen vacancies causes mutation of the barium titanate locally and also result in the reduction of the activation energy required for the injection of electrons from the cathode into the dielectric. This results in the degradation of leakage current [24].

All the above information is consistent with a lot of literature [19] [20] [21] [22] [23] [24], however, the mechanism for the degradation in the insulation resistance of the MLCCs under the presence of a varying voltage due to the varying voltage, which reverses the polarities of the MLCCs every half cycle. The oxygen vacancies cannot travel towards the cathode and accumulate near the Ni dielectric interface. But under the influence of an external varying voltage and the concentration gradient of defects, the oxygen vacancies can drift towards the grain boundaries, thus resulting in degradation of insulation resistance. To better understand the migration and relaxation of oxygen vacancies under the varying electric field, a popular method for the study of relaxation in defects was employed known as thermally stimulation polarization current.

3.2.1 Thermally Stimulated Depolarization Current

Thermally stimulated depolarization current studies are usually employed to characterize the response of dielectric as a function of temperature. The currents produced due to the relaxation of charges as a function of temperature are studied to characterize the dielectric material [52].

The standard procedure used to conduct the thermally stimulated depolarization current studies is as follows :

1. The sample is poled by placing it between the electrodes using an electric field (E_p) for a certain time duration t_p and at a temperature T_p
2. With the field still applied, the sample is cooled down to the temperature of interest. With the electric field removed, the temperature of the sample is then increased at a constant rate after shorting the sample
3. The current generated due to the relaxation of defects is constantly monitored as a function of temperature using a microammeter
4. The peaks obtained reveal information about the presence and the relaxation of defects in the dielectric

TSDC studies were used in previous studies to understand the migration and relaxation of oxygen vacancies in the bulk of barium titanate [53] [54] [55]. With barium titanate as the base material, the concentrations of Ho and Er to were changed to see the effects on the lifetimes of MLCCs under temperature DC bias testing. HALT was performed on the samples at a temperature of 150°C using an electric field of 25 V/μm. The testing was stopped when the leakage current increased ten times the initial value.

The failed samples obtained after the HALT were then used to perform thermally stimulated depolarization current analysis. The failed samples were polarized at a temperature of 130°C and at a DC bias of 25 V/μm. Later the polarizing field was removed, and the sample was shorted to allow the relaxation of transient charges. The temperature of the samples was then increased at a constant heating rate of 5°C/min while monitoring the leakage current, which was due to the relaxation of the oxygen vacancies.

Based on the current peaks obtained, a model for the relaxation of oxygen vacancies was proposed. Figure 35 shows the TSC plot obtained on HALT degraded sample as a function of temperature and different poling times and Figure 35 shows the model suggested for the redistribution of oxygen vacancies. With the increase in temperature, current peaks were observed at two different temperatures suggesting the relaxation of the charges in two stages. At the time of poling the capacitors, the positively charged oxygen vacancies travel towards the cathode and accumulate at the cathode/ceramic interface in the degraded sample. As the temperature of the sample is increased, a lower temperature (140°C) current peak was observed. The lower temperature current peak was attributed to the redistribution of the oxygen vacancies within the grains of barium titanate. At such low temperatures, the energy of the grain boundaries was larger than the energy of the oxygen vacancies, and as a result the oxygen vacancies cannot travel through the grain boundaries. The relaxation current decreases with the temperature as no more relaxation of the oxygen vacancies occurs. However, at temperatures over 220°C, the oxygen vacancies gain high enough energy to travel through the grain boundaries and redistribute themselves in the bulk of the dielectric [53]. This redistribution of oxygen vacancies throughout the dielectric causes the higher temperature peak. The proposed model was consistent with various other studies conducted on class II X7R MLCCs.

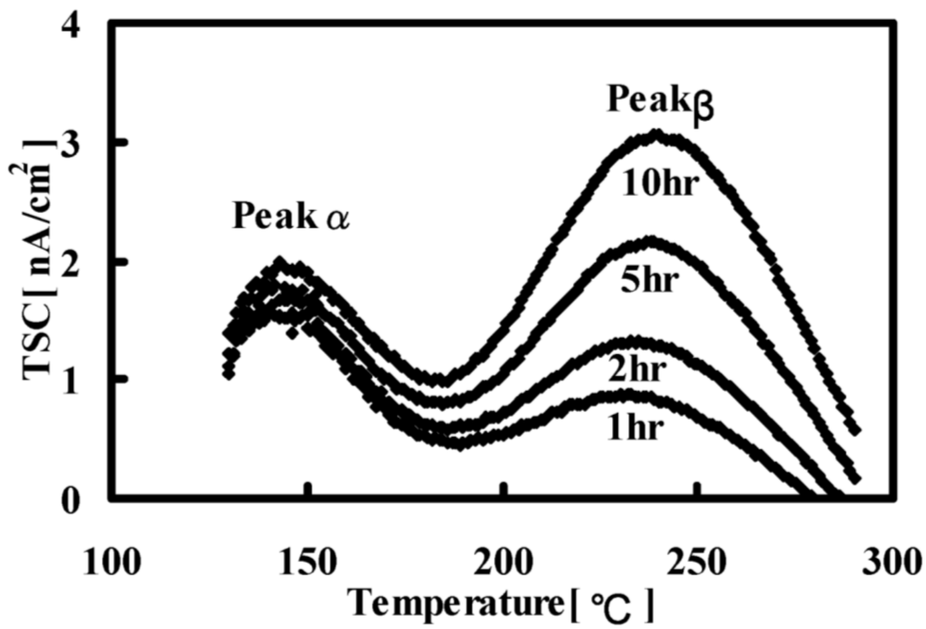

Figure 34 TSDC plot [53]

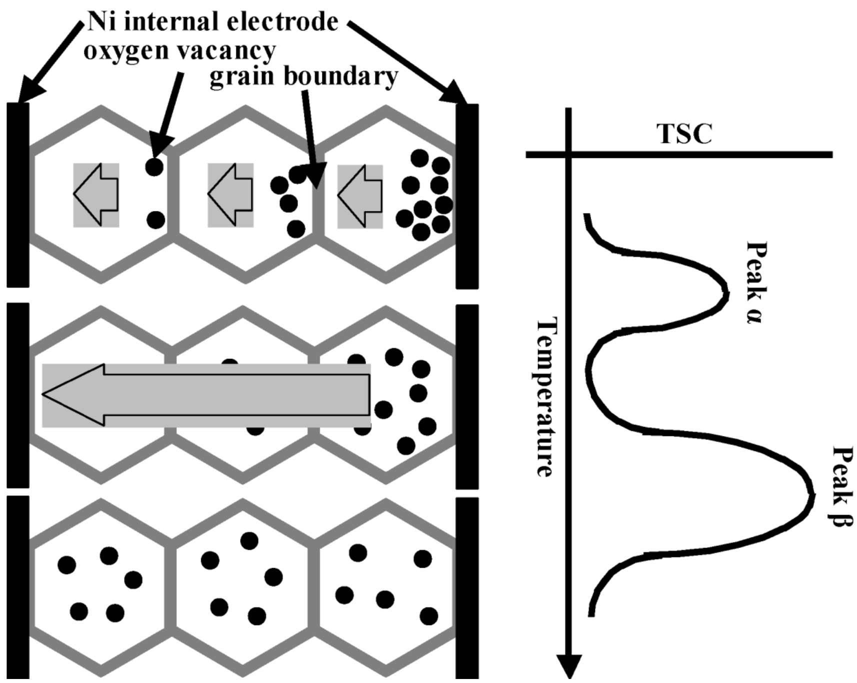

Figure 35 Model for relaxation of charges [53]

3.2.2 TSDC Analysis on Ripple Current Degraded Samples

TSDC was performed on a sample which degraded in insulation resistance from 18.8 GΩ to 2.89 GΩ under ripple current conditions. The TSDC plot was obtained by poling the sample at 130°C, 20 V for 30 minutes followed by increasing the temperature at a steady rate of 5°C/min after shorting the electrodes for 5 minutes. The maximum temperature was limited to 260°C because of the SMD board on which the MLCC was mounted.

Figure 36 shows the TSDC plot of the ripple current degraded sample. The TSDC plot obtained on the ripple current sample only had one lower temperature peak but not the higher temperature peak, unlike the HALT evaluated MLCCs. From the degradation model explained above, the cause of the lower temperature (140°C) peak can be attribute to the redistribution of the oxygen vacancies that diffused towards the cathode while poling the sample. At low temperatures, the redistribution of oxygen vacancies is limited to within the grain giving rise to the current peak as a function of temperature. However, unlike the HALT evaluated samples, no second peak was seen in the ripple current degraded samples.

The absence of the second peak can be explained by comparing the direction of externally applied electric field in the HALT evaluated samples and, in the ripple current degraded samples. In HALT testing, the direction of the externally applied electric field remains only in one direction throughout the duration of the testing. This causes the oxygen vacancies to diffuse only in one direction i.e., towards the cathode. But in the case of the ripple current tested samples, the direction of the externally applied electric field reverses the polarity for every half cycle and makes the diffusion of oxygen vacancies bidirectional in nature as opposed to the unidirectional diffusion of oxygen vacancies as opposed to the HALT tested samples.

The current observed in the HALT tested samples as a function of temperature is due to the relaxation of oxygen vacancies in one direction. However, in the ripple current samples, the bidirectional relaxation of oxygen vacancies as a function of temperature cancels out the current giving a net zero current. This explains the reason for the absence of the second peak in the ripple current degraded sample.

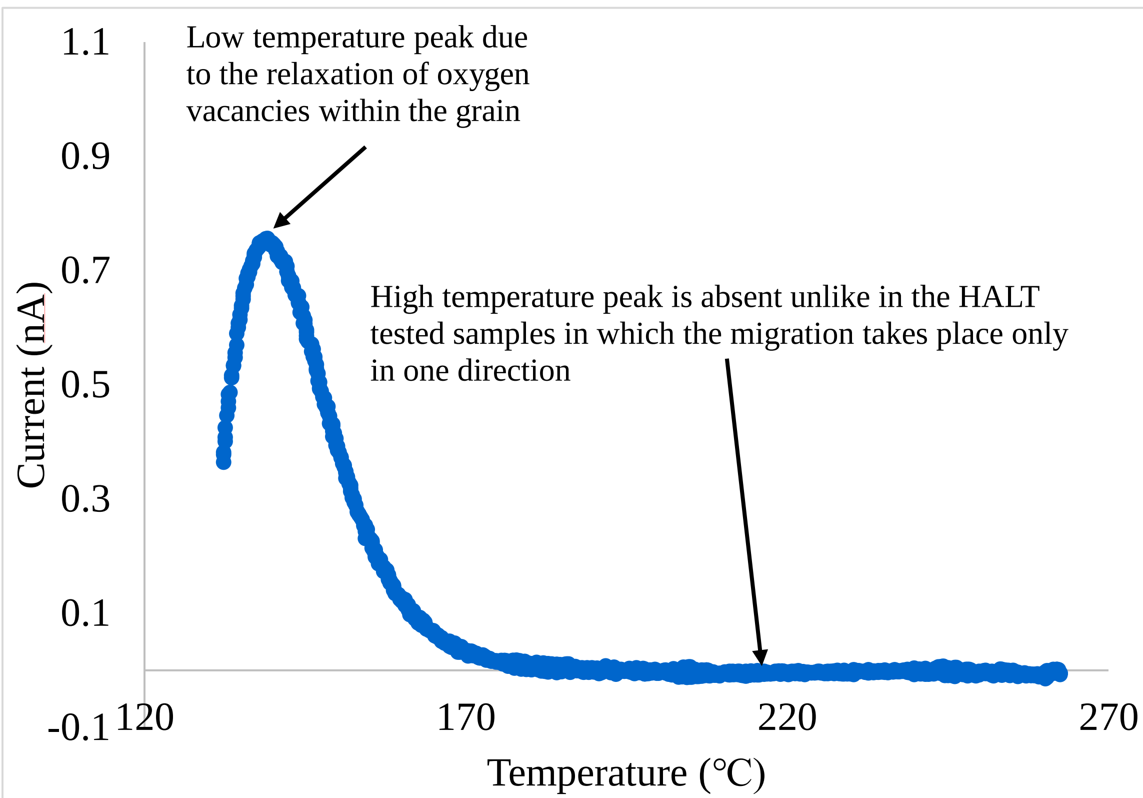

Figure 36 TSDC plot for ripple current degraded sample

In comparison, Figure 37 shows the TSDC plot for a new sample. The second peak does not exist in the TSDC plot for the new sample as well. The maximum of the lower temperature peak in the new sample is at 1 nA in comparison to the 0.725 nA in the degraded sample. The higher peak in the new sample suggests that the new sample had relatively a greater number of oxygen vacancies in comparison to the ripple current degraded sample. In the ripple current degraded sample, the oxygen vacancies might have drifted towards the grain boundaries or even getting trapped in them, resulting in a decrease in the number of available oxygen vacancies.

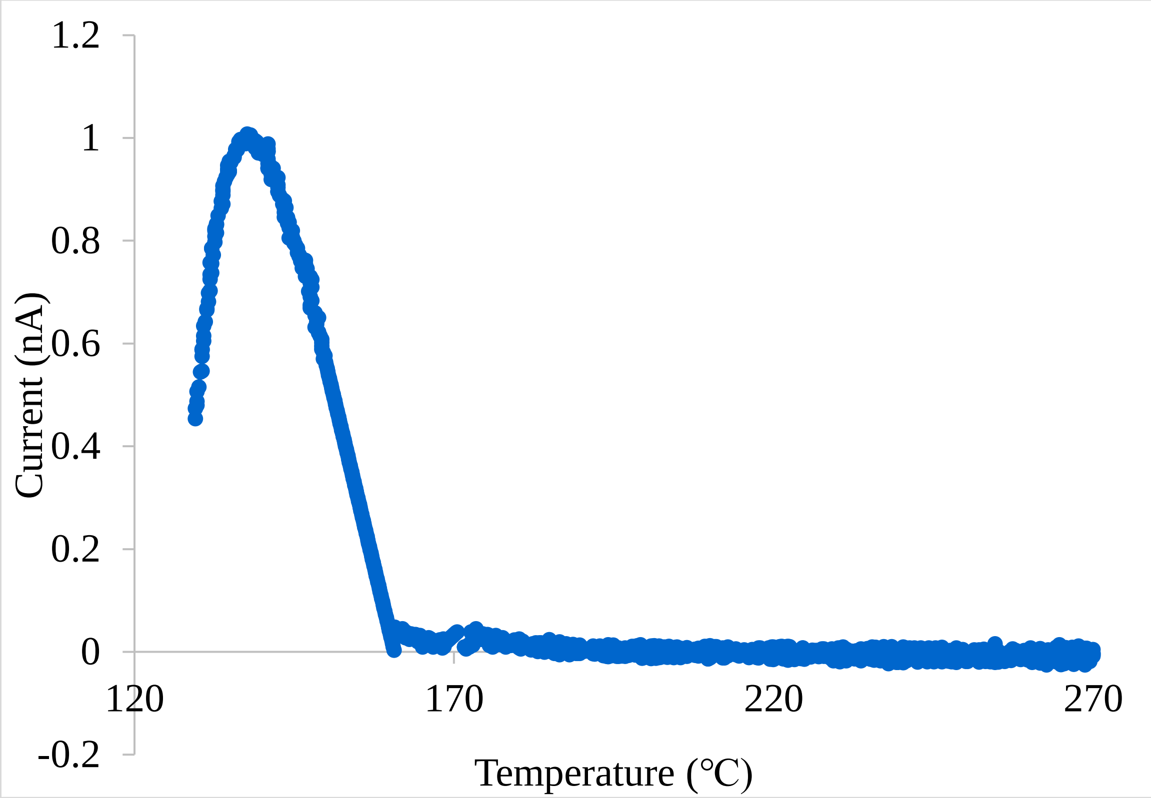

Figure 37 TSDC plot for new sample

3.2.3 Recovery of Insulation Resistance

Recovery in the insulation resistance of the ripple current degraded samples was observed after exposing them to a temperature of 250℃ for 30 minutes. The insulation resistance of a ripple current degraded sample recovered from 196 MΩ to 8.8 GΩ, which is close to its initial insulation resistance value.

The recovery in the insulation resistance of HALT degraded samples was also reported in some of previous studies [56] [57] [58]. The HALT testing was performed on samples at 250 ℃ using a DC field of 17 V. Testing was stopped when the rate of increase in leakage current of the samples reached an upper threshold of 0.003 mA/s. The insulation resistance of the sample decreased from 20 GΩ to 2 MΩ by the end of the HALT. The degraded samples were then baked at 300℃ for 10 minutes. The insulation resistance of the samples was reported to have recovered after the end of the baking procedure.

During HALT, the oxygen vacancies accumulate at the grain boundaries and at the ceramic/dielectric interface, causing insulation resistance degradation. At 300℃, the polarized oxygen vacancies redistribute themselves within the grain as well as through the bulk dielectric by diffusing through the grain boundaries [56] [57] [58]. This results in the recovery of the insulation resistance.

The recovery in the insulation resistance of the ripple current degraded samples can also be explained by the same phenomena of redistribution of localized oxygen vacancies.

3.3 Failure Mechanism in Ripple Current Degraded MLCCs

Degradation of insulation resistance can be caused either due to cracks or defect migration or a combination of both. Optical inspection of the degraded samples did not reveal any cracks on the external surface of the MLCCs. The recovery of the insulation resistance in the degraded samples on baking suggests the failure mechanism to be due to diffusion of oxygen vacancies into the grain boundaries. However, if an alternating electric field is applied on the MLCC, the net diffusion of the oxygen vacancies due to reversing electric field should be zero. Diffusion of oxygen vacancies in the presence of an electric field alone does not explain the theory of degradation due to oxygen vacancy migration.

The existence of the concentration gradient can help better explain the diffusion of oxygen vacancies under the influence of an externally applied AC field. In the dielectric, the core of the grain consists of pure barium titanate but on moving away from the core, modified barium titanate can be observed [3]. This is because of the added dopants in the barium titanate to modify the dielectric response in order to control the temperature dependence of the dielectric properties. The established core shell structure in the barium titanate creates a concentration gradient of defects within the grain [3] [28]. The core of the grain was reported to have high concentration of defects in comparison to the grain boundary regions.

With this available information, the diffusion of oxygen vacancies can be clearly understood. The imposition of an external alternating electric field over the concentration gradient of the defects, created net diffusion of the defects from the center of the grain towards the grain boundaries. The applied external electric field pulls the oxygen vacancies in the direction favorable both by the electric field as well as the concentration gradient. When the applied field and the concentration gradient are aligned in the same direction, the oxygen vacancies diffuse favorably in that direction. Reversing the direction of the electric field, antiparallel to the concentration gradient does not facilitate for the diffusion of oxygen vacancies. This results in a net diffusion of the oxygen vacancies from the center of the grain towards the grain boundaries resulting in the degradation of insulation resistance.

The restoration in the insulation resistance of the ripple current degraded samples after baking implies that the degradation is not permanent in nature. Degradation of the insulation resistance due to cracks would not allow for a full recovery in the insulation resistance because of the physical nature of the cracks. this showed that the mechanism for the degradation of insulation resistance can be attributed to the oxygen vacancy migration towards the grain boundaries.

4 Summary and Recommendations

MLCCs appear as a viable alternative to traditional electrolytic capacitors. But the lack of data on the performance of the MLCCs under varying voltage makes it hard to use MLCCs under ripple voltage conditions. A lot of research was done on the temperature and DC bias testing of MLCCs, and failure mechanisms were proposed regarding the degradation of insulation resistance. However, little is known about the performance and the lifetime of the MLCCs under varying voltage conditions and the applicability of the failure mechanisms seen in DC bias testing to the AC bias tested samples. AC testing causes current to flow through the capacitor and causes self-heating. Class II MLCCs also exhibit piezoelectric properties and under the influence of a varying electric field, it can undergo compression and elongation eventually leading to fatigue cracks. DC bias testing does not include the self-heating effects and the piezoelectric effects that are important for MLCCs working under ripple current conditions. The purpose of the study was to study the effects of ripple currents on the performance and on the lifetime of the MLCCs.

Ripple current tests were conducted on MLCCs with two different voltage ratings using an AC voltage and temperature as stress factors. Degradation in both the 6.3 V and the 16 V rated MLCCs was observed when evaluated under ripple current conditions. The possible degradation mechanism for the drop in insulation resistance can be attributed to the drifting of oxygen vacancies towards the grain boundaries, resulting in lowering the double Schottky barrier. Under the influence of the under the influence of the externally applied A/C field, the oxygen vacancies drift from the center of the grain towards the grain boundaries where they localize and lower the Schottky barrier potential. The lowered Schottky barrier potential allows for increased conductivity and results in lowering the insulation resistance of the MLCCs.

Surprisingly, no significant differences were seen in the performance of the 6.3 V and the 16 V rated MLCCs in spite of the 6.3 V operating at twice the rated voltage and with 16 V rated MLCC operating below its rated voltage. This suggests that the voltage ratings assigned for low voltage MLCCs may not consider the lifetimes of the MLCCs. However, this is speculation at this point, and quantification of lifetime is not possible from the tests due to a small sample size.

The average dielectric thickness was 8.4 µm for the 6.3 V rated MLCCs and 8.27 µm for the 16 V rated MLCCs. The electric field was 1.5V/µm on the 6.3 V MLCC and 1.52V/µm for the 16 V rated MLCC. The electric field on the MLCCs is an important parameter determining the lifetime of the MLCCs under the voltage stresses as the oxygen vacancy migration depends on the electric field applied on the dielectric. From the electric field, it can be seen that the 16 V rated MLCCs experienced slightly higher electric field in comparison to the 6.3 V rated MLCCs. The ineffectiveness of derating the 16 V rated sample can be associated to the higher electric field acting on the dielectric that resulted in drift of the oxygen vacancies towards the grain boundaries.

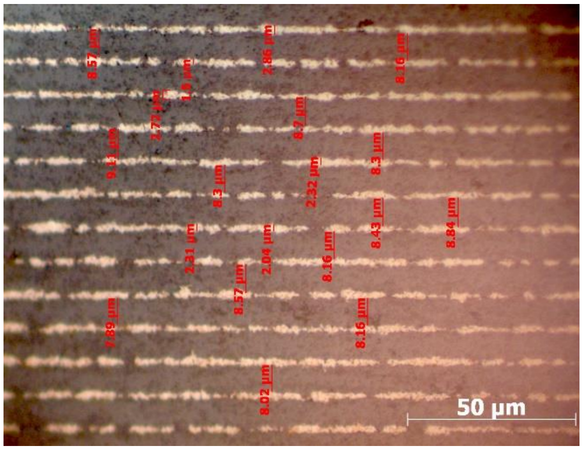

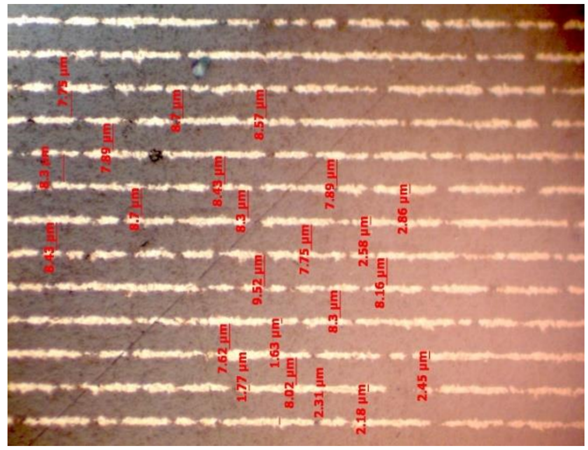

Figure 38 Cross section of 6.3 V MLCC

Figure 39 Cross section of 16 V MLCC

Recovery in the insulation resistance of the degraded samples on baking at 250℃ was seen, suggesting that the drop in insulation resistance is not permanent and that it can be reversed by baking them. Recovery in the insulation resistance of cracked MLCCs could not have been possible due to the physical nature of the crack (unless there was moisture ingress that got evaporated on heating).

However, the possibility of degradation due to cracking cannot be ignored due to the piezoelectric nature of the class II MLCCs. Previous study performed on MLCCs by operating them at their piezoelectric resonant frequency induced sever cracks on the body of the MLCCs. The piezoelectric resonant frequency of the MLCCs depends on the dimensions and care must be taken while selecting the case size of the MLCC to be used under ripple current conditions.

4.1 Derating Recommendations

Derating is a common practice used in the industry to enhance of the lifetime of the components by operating them below their rated specifications. At room temperatures, derating may not be required. A study performed on the relation between the voltage ratings and the breakdown voltages of the MLCCs revealed that the breakdown voltage is nearly 10 to 100 times the voltage ratings as assigned by the manufacturer [59]. Figure 40 shows the plot representing the relationship between the voltage rating and the break down voltages. It can be seen that the breakdown voltage of the 100 V rated MLCC is nearly 1000 V and for the 50 V rated MLCC the breakdown voltage varies anywhere from 300 V to 1000 V. A huge margin between the breakdown voltage and the voltage rating suggests that the voltage ratings may not have been assigned according to the breakdown voltages.

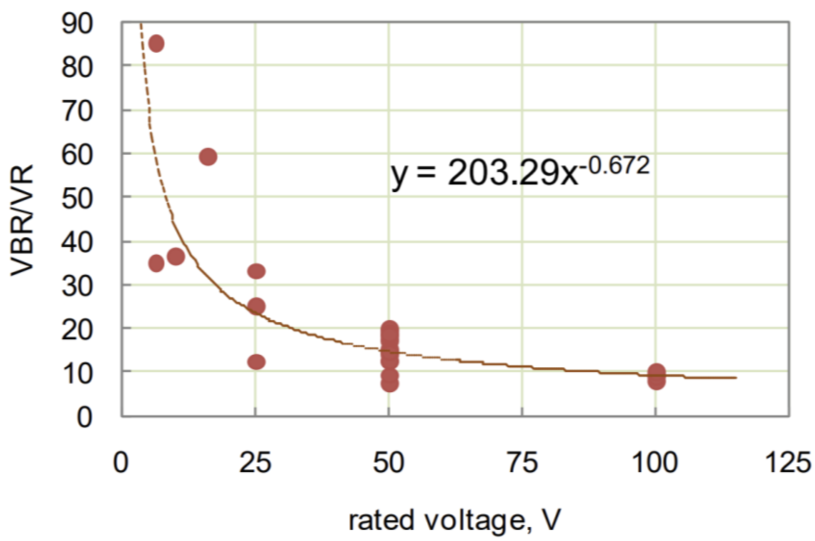

Figure 40 Breakdown voltage v/s voltage ratings [59]

The voltage ratings assigned by the manufacturers may be according to the polarization characteristics of the class II X7R MLCCs [49] [59]. The capacitance and the dissipation factor of the MLCCs is dependent on the applied DC bias. The capacitance and the dissipation factor of the MLCCs decrease with the increase in the applied DC bias due to the reduced randomization of the barium titanate domains. Figure 41 shows the alignment of domains with the applied DC bias. Figure 42 shows the change in capacitance of MLCCs (6.3 V and 16 V, 1206, 1 μF) with applied DC bias voltage.

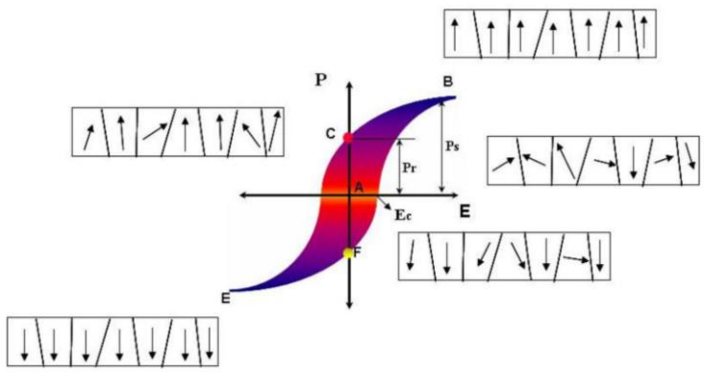

Figure 41 Hysteresis curve [60]

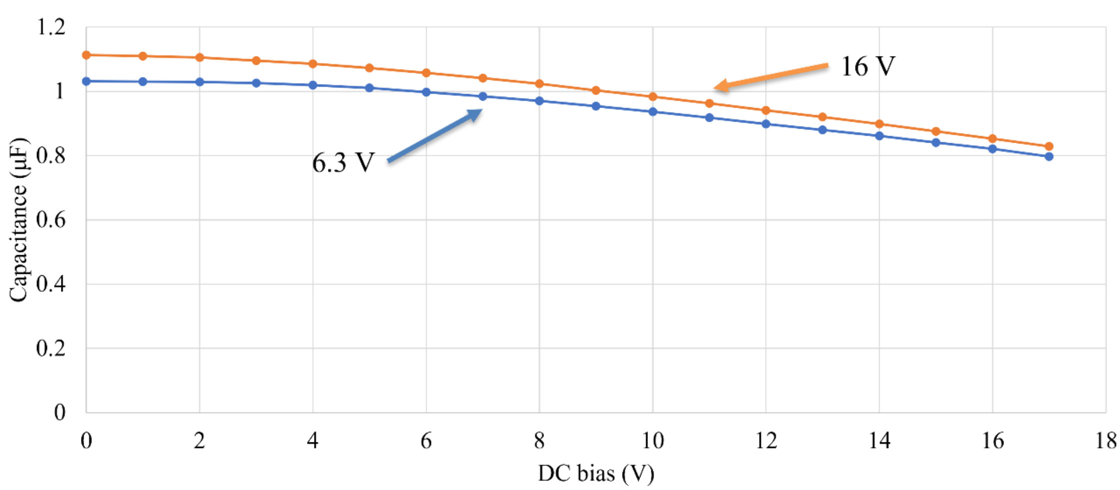

Figure 42 Capacitance v/s DC bias

However, at elevated temperatures, the mobility of the oxygen vacancies increases allowing them to diffuse towards the grain boundaries under the influence of an external electric field. Derating can be a useful tool to slow down the migration of oxygen vacancies while operating under elevated temperatures. Temperature due to both ambient conditions as well as due to self-heating must be considered while performing derating.

A common model used to estimate the lifetime of MLCCs, when the failure mechanism is due to oxygen vacancy migration, is by using the Prokopowicz and Vaskas equation [61] as mentioned below:

$$AF = \frac{\tau_1(V_1, T_1)}{\tau_2(V_2, T_2)} = \left(\frac{V_2}{V_1}\right)^n \times \exp\left[\frac{E_a}{k}\left(\frac{1}{T_1} - \frac{1}{T_2}\right)\right]$$

Equation 1 Prokopowicz and Vaskas model

where t_1 and t_2 are lifetimes, V_1 and V_2 are voltages, E_a is the activation energy, k is the Boltzmann constant, n is the voltage power law and T_1 and T_2 are the temperatures. The lifetime of the MLCCs can be calculated if the activation energy and the voltage power dependence is known.

In order to slow down the failures due to migration of oxygen vacancies and to increase the lifetime of the MLCCs, derating with respect to voltage and temperature can be used. The amount of derating depends on the values of n and E_a. MLCC manufacturers use different compositions of dopants to modify the dielectric properties to improve the temperature and DC bias properties of the MLCCs. A better understanding of the values of n and E_a can help better determine the level of derating required.

4.2 Conclusions

Ripple current testing performed on the X7R MLCCs resulted in the degradation of insulation resistance of the MLCCs. The degradation mechanism can be attributed to the diffusion of oxygen vacancies towards the grain boundaries, reducing the Schottky barrier height and thereby resulting in an increase in the conductivity of the dielectric. However, the possibility of cracking due to electrostriction should also be considered while operating at frequencies equal to the piezoelectric resonant frequencies of the poled MLCCs.

The performance and the lifetime of the MLCCs rated for different voltage ratings was evaluated in terms of the electric field acting on the dielectric material due to the externally applied ripple voltage. The 6.3 V rated MLCCs were overstressed (with respect to the rated voltage), whereas the 16 V rated MLCCs were derated (tested at 0.8*rated voltage). However, no significant difference in the lifetimes of the MLCCs were observed. The thinner dielectric on the 16 V rated MLCCs resulted in an electric field that was greater in magnitude in comparison to the 6.3 V rated MLCCs. Oxygen vacancy migration is dependent on the electric field acting on the dielectric material and thus governs the lifetime of the MLCC.

4.3 Contributions

1. The failure mode and the failure mechanism in Class II X7R MLCCs operating under ripple current conditions were identified.
    - Oxygen vacancy diffusion into the grain boundaries was identified as the failure mechanism in Class II X7R MLCCs that are operating under ripple voltage conditions and within their temperature limit, causing degradation of the insulation resistance
2. The effectiveness of derating the MLCCs with respect to voltage ratings, operating under ripple current conditions, was studied and an alternative method to derate the MLCCs was proposed
    - The electric field acting on the dielectric material influences the migration of the oxygen vacancies and thereby the lifetime of the MLCCs. Derating with respect to the voltage ratings was ineffective due to a higher electric field acting on the 16 V rated MLCCs in comparison to the 6.3 V rated MLCCs. Derating with respect to the electric field can be effective to slow the diffusion of oxygen vacancies and in extending the lifetime.

4.4 Future Work

The work conducted in this study is limited to testing only one manufacturer type and with no DC bias applied. In real world scenarios, a combination of both DC and AC bias would be applied on the MLCCs for filtering purposes. Testing the MLCCs using a combination of both DC bias and AC bias can be performed to check for any change in the degradation mechanism or the lifetimes. In addition, MLCCs from different manufacturers can be tested to better understand the performance and failures of MLCCs under ripple current conditions.

The samples used in this study was not large enough to quantify the failure times with acceptable confidence. The testing can be modified to increase the number of samples being tested in order to quantify the failure data and to make comparisons among MLCCs with different manufacturers and specifications.

Another interesting area of study would be to compare the performance and the lifetime of C0G MLCCs in comparison to the X7R MLCCs. Unlike the X7R MLCCs, the C0G MLCCs exhibit stable capacitance with respect to temperature, time, and DC bias. Also, the C0G MLCCs do no exhibit any electrostriction properties making it immune to failure due to cracking when an external field is applied (still susceptible to flex cracking). Failures due to oxygen vacancy migration are also not found in the C0G MLCCs under HALT conditions. C0G MLCCs are the recommended capacitor types for applications involving ripple voltages due to above mentioned reasons, however, the long-term reliability of the C0G must be experimentally verified.

5 References

[1] J. Tahalyani, M. J. Akhtar and K. K. Kar, "Characteristics of Capacitor: Fundamental Aspects," in *Handbook of Nanocomposite Supercapacitor Materials I*, Springer, Cham, 2020, pp. 1-51.

[2] "What is the role of a Capacitor in Electronic Components? Focusing on the mechanism," Matsusada Precision Inc., 18 March 2020. [Online]. Available: https://www.matsusada.com/column/capacitor.html.

[3] M.-J. Pan and C. A. Randall, "A brief introduction to ceramic capacitors," *IEEE Electrical Insulation Magazine,* vol. 26, no. 3, pp. 44-50, 2010.

[4] B. Brunette, "The Basics & Benefits of Tantalum & Ceramic Capacitors," 2018.

[5] L. Smith, T. Ibn Mohammed, S. L. Koh and I.M. Reaney, "Life cyccle assesment and environmental profile evaluations of high volumetric efficiency," *Applied Energy,* vol. 220, pp. 496-513, 2018.

[6] H. Takahasi, "A note on the theory of barium titanate," *Journal of the Physical Society of Japan,* vol. 16, no. 9, pp. 1685-1689, 1961.

[7] P. W. Forsbergh, "Domain Structures and Phase Transitions in Barium Titanate," *American Physical Society,* vol. 76, no. 8, pp. 1187-1201, 1949.

[8] A. von Hippel, "Ferroelectricity, Domain Structure, and Phase Transitions of Barium Titanate," *Reviews of Modern Physics,* vol. 22, no. 3, pp. 221-237, 1950.

[9] M. B. Smith, K. Page, T. Siegrist, P. L. Redmond, E. C. Walter, R. Seshadri, L. E. Brus and M. L. Steigerwald, "Crystal Structure and the Paraelectric-to-Ferroelectric Phase Transition of Nanoscale BaTiO3," *Journal of the American Chemical Society,* vol. 130, no. 22, pp. 6955-6963, 2008.

[10] Q. Wang, H.-Z. Yan, X. Zhao and C.-M. Wang, "Polymorphic Phase Transition and Piezoelectric Performance of BaTiO3-CaSnO3 Solid Solutions," *MDPI,* vol. 129, p. 10, 2021.

[11] D. Neumayr, D. Bortis, J. W. Kolar, M. Koini and J. Konrad, "Comprehensive large-signal performance analysis of ceramic capacitors for power pulsation buffers," in *2016 IEEE 17th Workshop on Control and Modeling for Power Electronics (COMPEL)*, Trondheim, Norway, 2016.

[12] N. Musarrat, R. Islam, K. M. Muttaqi and D. Sutanto, "Shunt Active DC Filter to Reduce the DC Link Ripple Current Caused by Power Converters to Improve the Lifetime of Aluminium Electrolytic Capacitor," in *2020 IEEE Industry Applications Society Annual Meeting*, Detroit, MI, USA, 2020.

[13] J. Huang, Y. Wan, C. Gao and Y. Xiong, "Discussion on multilayer ceramic replacements for tantalum capacitors," in *2015 Prognostics and System Health*

Management Conference (PHM), 2015.

[14] J. Both, "The modern era of aluminum electrolytic capacitors," *IEEE Electrical Insulation Magazine,* vol. 31, no. 4, pp. 24-34, 2015.

[15] L. Smitha, T. Ibn-Mohammed, S. L. Koh and I. M. Reaneya, "Life cycle assessment and environmental profile evaluations of high volumetric efficiency capacitors," *Applied Energy,* vol. 220, pp. 496-513, 2018.

[16] H. Takamizawa, K. Utsumi, M. Yonezawa and T. Ohno, "Large Capacitance Multilayer Ceramic Capacitor," *IEEE Transactions on Components, Hybrids, and Manufacturing Technology,* vol. 4, no. 4, pp. 345-349, 1981.

[17] S. Somiya, "Ceramics," in *Encyclopedia of Physical Science and Technology (Third Edition)*, Academic Press, 2003, pp. 569-619.

[18] J. Huang, Y. Wan, C. Gao and Y. Xiong, "Discussion on multilayer ceramic replacements for tantalum capacitor," in *2015 Prognostics and System Health Management Conference (PHM)*, Beijing, 2015.

[19] G. Y. Yang, G. D. Liana, E. C. Dickey and C. A. Randall, "Oxygen nonstoichiometry and dielectric evolution of BaTiO3. Part II—insulation resistance degradation under applied dc bias," *Journal of Applied Physics,* vol. 96, no. 12, pp. 7500-7508, 2004.

[20] T. Sada and N. Fujikawa, "Analysis of insulation resistance degradation in Ni–BaTiO3 multilayer ceramic capacitors under highly accelerated life test," *Japanese Journal of Applied Physics,* vol. 10PB04, p. 56, 2017.

[21] Saito, Yoshito, T. Nakamura, K. Nada and H. Sano, "Insulation resistance degradation mechanisms of multilayer ceramic capacitors during highly accelerated temperature and humidity stress tests," *Japanese Journal of Applied Physics,* vol. 57, no. 11S, p. 11UC04, 2018.

[22] T. Okamoto, S. Kitagawa, N. Inoue and A. Ando, "Electric field concentration in the vicinity of the interface between anode and degraded BaTiO3-based ceramics in multilayer ceramic capacitor," *Applied Physics Letters,* vol. 98, no. 7, 2011.

[23] J. Kim, D. Yoon, M. Jeon, D. Kang, J. Kim and H. Lee, "Degradation behaviors and failure analysis of Ni–BaTiO3 base-metal electrode multilayer ceramic capacitors under highly accelerated life test," *Current Applied Physics,* vol. 10, no. 5, pp. 1297-1301, 2010.

[24] D. D. Liu, "Insulation Resistance Degradation in Ni–BaTiO3 Multilayer Ceramic Capacitors," *IEEE Transactions on Components, Packaging and Manufacturing Technology,* vol. 5, no. 1, pp. 40-48, 2015.

[25] C. B. Barth, T. Foulkes, I. Moon, Y. Lei, S. Qin and R. C. N. Pilawa-Podgurski, "Experimental Evaluation of Capacitors for Power Buffering in Single-Phase Power

Converters," *IEEE Transactions on Power Electronics,* vol. 34, no. 8, pp. 7887-7899, 2019.

[26] C. Lee and J. Yoon, "Finite Element Analysis of Multi-Layer Ceramic Capacitors Improved Self-heating for High Reliability," *Transactions on Electrical and Electronic Materials,* vol. 22, pp. 424-431, 2021.

[27] S. Coday and R. C. Pilawa-Podgurski, "High Accuracy Calorimetric Measurements and Modeling of Ceramic Capacitor Losses Under Large Ripple Operation," in *2020 IEEE Applied Power Electronics Conference and Exposition (APEC),* New Orleans, LA, USA, 2020.

[28] W. A. SCHULZE, L. E. CROSS and W. R. BUESSEM, "Degradation of BaTiO3 Ceramic Under High ac Electric Field," *Journal of the American Ceramic Society,* vol. 63, no. 1-2, pp. 83-87, 1980.

[29] K. Wu and W. A. Schulze, "Effect of the AC Field Level on the Aging of the Dielectric Response in Polycrystalline BaTiO3," *Journal of American Ceramic Society*, vol. 75, no. 12, pp. 3385-3389, 1992.

[30] "Application Note | Ripple Current and MLCC: Basic Principles," Kemet, 4 May 2021. [Online]. Available: https://ec.kemet.com/blog/ripple-current-and-mlcc-basic-principles/.

[31] X. Xu, M. Niskala, A. Gurav, M. Laps, K. Saarinen, A. Tajuddin, D. Montanari, F.

Bergamaschi and E. Boni, "Advances in class-I C0G MLCC and SMD film capacitors," in *Proceedings of the 28th Symposium for Passive Components (CARTS USA 2008)*, Newport Beach, 2008.

[32] D. (. Liu, "Part II: Evaluation of Multilayer Ceramic Capacitors with C0G Dielectric and Base-Metal Electrodes," NASA Electronic Parts and Packaging Program , 8800 Greenbelt Road , 2012.

[33] L. D. Madsen and E. B. Svedberg, "KEMET Electronics: Breakthroughs in Capacitor Technology," in *Materials Research for Manufacturing*, Springer, 2016, p. 108.

[34] V. Buscaglia, M. T. Buscaglia and G. Canu, "BaTiO3-Based Ceramics: Fundamentals, Properties and Applications," in *Encyclopedia of Materials: Technical Ceramics and Glasses*, Elsevier, 2021, pp. 311-344.

[35] R. Sharma, R. Singh and A. Batish, "Investigations for Barium Titanate and Graphene Reinforced PVDF Matrix for 4D Applications," in *Encyclopedia of Renewable and Sustainable Materials*, Elsevier, 2020, pp. 366-375.

[36] N. M. J. Li, *Effects of Ferroelectric Properties on Mechanical Behavior of Class II Multilayer Ceramic Capacitors,* Doctoral dissertation, 2019.

[37] P. R. Potnis, N.-T. Tsou and J. E. Huber, "A Review of Domain Modelling and Domain Imaging Techniques in Ferroelectric Crystals," *Materials (Basel),* vol. 4, no.

2, pp. 417-447, 2011.

[38] R. C. BRADT and G. S. ANSELL, "Aging in Tetragonal Ferroelectric Barium Titanate," *Journal of American Ceramic Society,* vol. 52, no. 4, pp. 192-198, 1969.

[39] L. Mitoseriu, V. Tura, M. Curteanu, D. Popovici and A. Anghel, "Aging effects in pure and doped barium titanate ceramics," *IEEE Transactions on Dielectrics and Electrical Insulation,* vol. 8, no. 3, pp. 500-506, 2001.

[40] W. A. Schulze and K. Ogino, "Review of literature on aging of dielectrics," *Ferroelectrics,* vol. 87, no. 1, pp. 361-377, 1988.

[41] M. M. Ahmad and K. Yamada, "Aging-induced dielectric relaxation in barium titanate ceramics," *Applied Physics Letters,* vol. 90, no. 11, 2007.

[42] muRata, [Online]. Available: https://www.murata.com/en-eu/support/faqs/capacitor/ceramiccapacitor/char/0006.

[43] M. Keimasi, M. H. Azarian and M. G. Pecht, "Flex Cracking of Multilayer Ceramic Capacitors Assembled With Pb-Free and Tin–Lead Solders," *IEEE Transactions on Device and Materials Reliability,* vol. 8, no. 1, pp. 182-192, 2008.

[44] N. Blattau, D. Barker and C. Hillman, "Lead free solder and flex cracking failures in ceramic capacitors," in *CARTS-CONFERENCE*, 2004.

[45] J. F. Soeder, R. J. Scheidegger, L. R. Pinero, A. J. Birchenough and J. W. Dunning,

"NASA's Evolutionary Xenon Thruster (NEXT) Power Processing Unit (PPU) Capacitor Failure Root Cause Analysis". Atlanta, GA Patent NASA/TM-2012-217667, 1 August 2012.

[46] D. Zhang, T. Hubing, A. Ritter and C. Nies, "The Effect of Electrical Fast Transients on Multi-Layer Ceramic Capacitors," *IEEE Trans. on Components, Packaging and Manufacturing Technology,* vol. 6, no. 4, pp. 553-560, 2015.

[47] B. C. Sekhar, B. Dhanalakshmi, B. S. Rao, S. Ramesh, K. V. Prasad, P. S. Rao and B. P. Rao, "Piezoelectricity and Its Applications," in *Multifunctional Ferroelectric Materials*, London, United Kingdom, 2021.

[48] A. El-amiri, H. Mokhliss, A. Saifi, H. Halloua, A. Obbadi, Y. Errami, S. Sahnoun and A. Elhassnaoui, "Infrared Thermography Detection of Flex Cracks in Multi-Layer Ceramic Capacitors (MLCCs)," in *2018 6th International Renewable and Sustainable Energy Conference (IRSEC)*, Rabat, Morocco, 2018.

[49] A. Teverovsky, "Guidelines for Selection, Screening and Qualification of Low-Voltage Commercial Multilayer Ceramic Capacitors for Space Programs," 2012.

[50] K. Nishida, H. Kishi, H. Funakubo, H. Takeuchi, T. Katoda and T. Yamamoto, "Evaluation of Residual Strain and Oxygen Vacancy in Multilayer Ceramic Capacitor Using Laser Raman Spectroscopy," *Japanese Journal of Applied Physics,* vol. 46, no. 10S, p. 7005, 2007.

[51] D. Brown, "Oxygen vacancy migration in MLCCS," *Pan Pacific Microelectronics Symposium (Pan Pacific)*, pp. 1-6, 2018.

[52] P. Pissis, S. Kripotou and A. Kyritsis, "7 - Dielectric relaxation in polymer–clay nanocomposites," in *Physical Properties and Applications of Polymer Nanocomposites*, Woodhead Publishing, 2010, pp. 247-279.

[53] S. Takeoka, K. Morita, Y. Mizuno and H. Kishi, "Thermally Stimulated Current (TSC) Studies on Resistance Degradation of Ni-MLCC," *Ferroelectrics*, vol. 356, pp. 78-84, 2007.

[54] K. Morita, Y. Mizuno and H. Chazono, "Degradation of Resistance over Time for Multilayer Ceramic Capacitors," *Key Engineering Materials* , vol. 445 , p. 35–38, 2010.

[55] W. Wu, Z. Liu, Y. Gu, Z. Yue and Y. Li, "Thermally stimulated depolarization current study on barium titanate single crystals," *AIP Advances* , vol. 8, no. 4, p. 045005, 2018.

[56] T. Sada and N. Fujikawa, "Analysis of insulation resistance degradation in Ni–BaTiO3 multilayer ceramic capacitors under highly accelerated life test," *Japanese Journal of Applied Physics*, vol. 56, no. 10S, 2017.

[57] S.-H. Yoon, C. A. Randall and K.-H. Hur, "Correlation Between Resistance Degradation and Thermally Stimulated Depolarization Current in Acceptor (Mg)-

Doped BaTiO3 Submicrometer Fine-Grain Ceramics," *Journal of the American Ceramic Society,* vol. 93, no. 7, pp. 195-1956, 2010.

[58] "Charge Carrier Relaxation Study in Glass-Added Barium Titanate Ceramics Using Thermally Stimulated Depolarization Current," *Journal of Electronic Materials,* vol. 45, pp. 4044-4051, 2016.

[59] A. Teverovsky, "Breakdown voltages in ceramic capacitors with cracks," *IEEE Transactions on Dielectrics and Electrical Insulation,* vol. 19, no. 4, pp. 1448-1455, 2012.

[60] D. Brown, "Multilayer Ceramic Capacitors : Mitigating Rising Failure Rates," 2017.

[61] T.I.Prokopowicz and A.R.Vaskas, "Research and development intrinsic reliability subminiature ceramic capacitors,," Final Report, ECOM-90705-F,1969 NTIS AD-864068, 1969.